ELECTRON IMPACT IONIZATION CROSS SECTIONS OF GOLD, CHROMIUM AND IRON

MASSACHUSETTS INSTITUTE OF TECHNOLOGY

JANUARY 1976

AFML-TR-75-198

ELECTRON IMPACT IONIZATION CROSS SECTIONS OF GOLD, CHROMIUM AND IRON

Avi N. Nelson
Massachusetts Institute of Technology
77 Massachusetts Avenue
Cambridge, Massachusetts 02139

March, 1976

TECHNICAL REPORT AFML-TR-75-198

Final Report for Period 16 April 1971 - 31 December 1973

Approved for public release, distribution unlimited.

AIR FORCE MATERIALS LABORATORY
AIR FORCE WRIGHT AERONAUTICAL LABORATORIES
AIR FORCE SYSTEMS COMMAND
WRIGHT-PATTERSON AIR FORCE BASE, OHIO 45433

UNCLASSIFIED

SECURITY CLASSIFICATION OF THIS PAGE (When Data Entered)

REPORT DOCUMENTATION PAGE	READ INSTRUCTIONS BEFORE COMPLETING FORM
1. REPORT NUMBER: AFML-TR-75-198	2. GOVT ACCESSION NO. / 3 RECIPIENT'S CATALOG NUMBER
4. TITLE (and Subtitle): Electron Impact Ionization Cross Sections of Gold, Chromium and Iron	5. TYPE OF REPORT & PERIOD COVERED: Final Tech. Report 16 Apr 71 - 31 Dec 73
	6 PERFORMING ORG. REPORT NUMBER
7 AUTHOR(s): Avi N. Nelson	8 CONTRACT OR GRANT NUMBER(s): F33615-71C-1420 New
9 PERFORMING ORGANIZATION NAME AND ADDRESS: Massachusetts Institute of Technology Cambridge, MA 02139	10 PROGRAM ELEMENT, PROJECT, TASK AREA & WORK UNIT NUMBERS: Project 7367 Task 736704
11. CONTROLLING OFFICE NAME AND ADDRESS	12 REPORT DATE: Jan 76
	13 NUMBER OF PAGES: 96
14 MONITORING AGENCY NAME & ADDRESS (if different from Controlling Office): Air Force Wright Aeronautical Laborato Air Force Materials Laboratory AFML/LPJ Wright Patterson AFB, OH 45433	15 SECURITY CLASS. (of this report): UNCLASSIFIED
	15a DECLASSIFICATION/DOWNGRADING SCHEDULE

16. DISTRIBUTION STATEMENT (of this Report)

Approved for public release, distribution unlimited.

17 DISTRIBUTION STATEMENT (of the abstract entered in Block 20, if different from Report)

18 SUPPLEMENTARY NOTES

19. KEY WORDS (Continue on reverse side if necessary and identify by block number)

Cold
Chromium
Iron
Mass Spectrometry

20 ABSTRACT (Continue on reverse side if necessary and identify by block number)

Relative and absolute electron impact ionization cross sections were measured for species of three elements. The data include results on Au^{+}, Au^{2+}, Au^{3+}; Cr^{+}, Cr^{2+}; Fe^{+}, Fe^{2+}, Fe^{3+}. Total cross section results on the elements are also reported.

A description of the procedure and equipment as well as some of the difficulties in the experiment are presented.

Related information from the literature, both experimental and theoretical, are discussed in a comparative context.

DD FORM 1 JAN 73 1473 EDITION OF 1 NOV 65 IS OBSOLETE

UNCLASSIFIED

ELECTRON IMPACT IONIZATION CROSS SECTIONS OF GOLD, CHROMIUM AND IRON

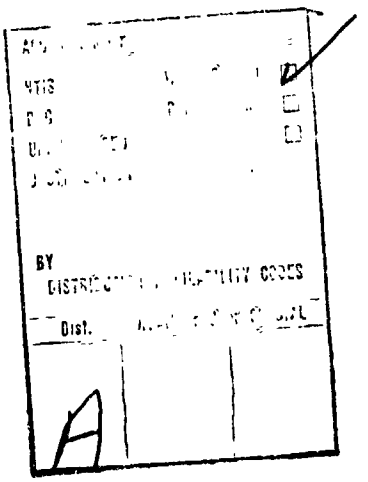

Approved for public release, distribution unlimited.

PREFACE

This report was prepared by Massachusetts Institute of Technology, Cambridge, MA 02139, under USAF Contract No. F33615-71-C-1420. This contract was initiated under Project No. 7367, "Research on Characterization and Properties of Materials for Air Force Systems," Task No. 736704, "Materials Degradation in Unique Environments." The work was administered under the direction of the Air Force Materials Laboratory, Air Force Systems Command, Wright-Patterson Air Force Base, OH, with Mr. Paul W. Dimiduk, (AFML/LPJ) as Technical Monitor. Funds for this project were supplied to the AF Materials Laboratory by the Office of Aerospace Research.

Work covered by this report was carried out from 16 April 1971 through 31 December 1973. The report was submitted by Massachusetts Institute of Technology in October 1975 for publication as an AFML Technical Report.

The author wishes to acknowledge the technical and experimental help given by Dr. C.K. Crawford and Dr. K.L. Wang. Also, thanks are due to John Mara who did the drawings and Janice Davis who typed the manuscript.

This technical report has been reviewed and is approved for publication.

Paul W. Dimiduk

PAUL W. DIMIDUK
Project Monitor

Paul W. Elder

PAUL W. ELDER, MAJOR, USAF
Chief, Laser Hardened Materials Branch
Air Force Materials Laboratory

NOTICE

When Government drawings, specifications, or other data are used for any purposes other than in connection with a definitely related Government procurement operation, the United States Government thereby incurs no responsibility nor any obligation whatsoever; and the fact that the government may have formulated, furnished, or in any way supplied the said drawings, specifications, or other data, is not to be regarded by implication or otherwise as in any manner licensing the holder or any other person or corporation, or conveying any rights or permission to manufacture, use, or sell any patented invention that may in any way be related thereto.

This report has been reviewed by the Information Office (OI) and is releasable to the National Technical Information Service (NTIS). At NTIS, it will be available to the general public, including foreign nations.

Copies of this report should not be returned unless return is required by security considerations, contractual obligations, or notice on a specific document.

TABLE OF CONTENTS

LIST OF ILLUSTRATIONS

1.0 INTRODUCTION

1.1 General Background

Cross sections are important in the study of mass spectrometry, space physics, plasmas and in providing an experimental check on some of the approximations of quantum theory. In recent years, however, comparatively few direct measurements of absolute cross sections have been undertaken. This is due partly to the sophisticated and expensive equipment required for accurate results and partly to the narrow amount of information that can be gleaned from the rather large investment. More data of a relative nature have been produced and these often "absolutized" by affixment to a chosen standard.

This report presents the results of experimentation on three metals. The absolute cross sections were measured as a function of electron bombardment energy for single and multiple ionization processes for each of the elements. The subjects chosen were gold, chromium and iron, because they are relatively important in usage and moderately difficult in terms of handling.

Another factor in the selection was the oxidation characteristics of the elements. The nature of the investigation requires evaporation of the experimental material in order to create an atomic beam. Some of the beam, of necessity, intersects and deposits on certain

electrode surfaces in the vacuum envelope. This is not part of the experiment itself, but short of major design modifications in the internal structure, is an expected consequence of the procedure. If the deposit is easily oxidized when exposed to air, the electrodes will become coated with an insulating layer which grossly distorts the desired electric field pattern. Mg is an example of a material which behaves in such a way forming non-conductive MgO. This particular problem was not faced in the course of the present investigation, because Au, Cr and Fe deposits do not form insulating oxides in dry air.

The moderate difficulty is a reference to the pressure-temperature characteristics of the metals. They are in a group below the refractory materials while still falling significantly above the high vapor pressure elements. The latter are much more amenable to this kind of experimentation, as emphasis in the cross section literature indicates. This explains the comparative sparseness of results with regard to the three metals discussed here.

In the case of gold, there was one prior reported determination of absolute results. Cr and Fe have never been directly measured before, although some relative experiments have been performed.[1,3,4,9]

1.2 Cross Section Equation

A billiard ball model of the interaction between an electron beam and an atom gas leads to the basic form of the cross section equation. Consider a gas of density N atoms/cm^3 and per atom cross sectional area of A cm^2. The chance of an electron colliding with an atom within a small length L is NAL so long as N and L are small.

If there is an electron beam of current I, the amount of loss of beam current ΔI over a distance L is

$$\Delta I = NALI$$

In this case, the cross section is simply the projected area of the atomic sphere. In reality, of course, the interaction is electrostatic, and the atomic particles must be treated as wave packets.

It is this quantum mechanical description which leads to a finite total cross section. It can be shown that finiteness prevails when the interaction force goes as $1/r^m$ where $m > 3$ for large r.[22]

Also, the cross section is dependent upon the electron velocity and on the type of collision under investigation. For the case of ionization, the

different collision possibilities are the different orders of ionization which can result. In order to represent this more sophisticated cross section concept, the conventional σ is used with a superscript designation of species.

Thus, the total cross section equation is

$$I_i = NIL\sigma,$$

and in species form

$$I_i^{+} = NIL\sigma^{+}$$

$$I_i^{2+} = NIL\sigma^{2+}$$

$$\vdots \qquad \vdots$$

$$I_i^{n+} = NIL\sigma^{n+}$$

Now in practical terms ΔI is five or six orders of magnitude below I. This makes for great difficulty in measuring the change in current by collection of the relatively few "lost" electrons, because of the proximity and magnitude of the main beam.

One way around this is to measure the ion current, since each ion represents a single electron

collision and removal of that electron from the beam. It must be recalled, however, that not all ions carry the same charge or contribute to the current in the same way. Each ion component must be weighted by its charge.

Denoting an ion current (as opposed to an electron current) by a subscript i, we have

$$I_i = I_i^+ + I_i^{2+} + \ldots + I_i^{n+}$$

In order to equate this to an electron current, it is necessary to divide out the effect of multiple charges. Then

$$\Delta I = \Delta I^+ + \Delta I^{2+} + \ldots + \Delta I^{n+} = I_i^+ + \frac{I_i^{2+}}{2} + \ldots + \frac{I_1^{n+}}{n}$$

Since there is a one to one correspondence between the equations,

$$I_i^+ = \Delta I^+ = NIL\sigma^+$$

$$I_i^{2+} = 2\Delta I^{2+} = 2NIL\sigma^{2+}$$

$$\vdots \qquad \vdots \qquad \vdots$$

$$I_i^{n+} = n\Delta I^{n+} = nNIL\sigma^{n+}$$

thus

$$I_i = NIL \sum_{k=1}^{n} k\sigma^{k+} = NIL\sigma$$

where

$$\sigma = \sum_{k=1}^{n} k\sigma^{k+}$$

In this investigation $n \leq 3$, and higher orders are negligible in contribution to the total cross section.

2.0 GENERAL DESCRIPTION

2.1 System

The experimental system was designed to provide an empirical solution to the equation

$$\sigma = \frac{I_i}{NLI_e} \quad .$$

In this regard, it was necessary to be able to measure accurately the ion current resulting from the intersection of measurable atomic and electron beams over a known interaction path.

The neutral density N was derived from the physics of an atomic beam generated in an evaporation-type source. The electron current, I_e, was created with an electron gun configuration. The interaction length, L, was a fixed quantity directly related to the internal geometry of the chamber wherein beam interaction occured. The ion current, I_i, was detected by collection both in total and species form - the latter requiring selection and particularization. Each of the above sub-system functions is discussed in subsequent sections of this report.

The constraints of the experiment required that operation be conducted in a vacuum. The vacuum envelope enclosed approximately a 20 liter volume which was evacuated by a Welch Scientific Duo Seal Model 1397 500 lpm

mechanical rough pump and a NRC VHS-4 4" oil diffusion pump in tandem. A Granville-Phillips liquid nitrogen trap was added system-side to condense back streaming oil before contamination of vacuum surfaces resulted. As is explained later, however, the problem of contamination was not so easily resolved.

With only the vacuum system in operation pressures as low as 3×10^{-8} Torr were not unusual. With the atom source operating also, the pressure climbed often onto the seven scale. Ordinarily, the system ran during experimental conditions in the range $4 \times 10^{-8} \leq P \leq 2 \times 10^{-7}$ Torr.

The basic theory of the experiment was to direct mutually orthogonal atomic and electron beams into an intersection region. As the electron beams impinged on the beam of neutrals, some of the atoms became ionized. These ions were drawn off along the third orthogonal axis either for total collection or for species selection in a mass spectrometer.

The output of the spectrometer was amplified in an electron multiplier, appropriately processed, and displayed on either an x-y recorder or a digital voltmeter.

2.2 Electron Gun

The genesis of the electron beam was accomplished by means of a modified einzel lens configuration set between a filament-extration electrode assembly and a Faraday cup collector. The ionization chamber in which the beam interaction occurs was located between the lens and the collector.

Electrons were emitted by a 125μ W-Re (3%) filament which evolved in shape from a basic hairpin design to a modified "W" form. In fact, the filament looks like a "W" with the two outer legs bent down at the mid-points and gripped at the ends. The reason for the modification was to provide additional length to the filament and thus reduce some of the thermal conduction loss.[2]

The apex or center of the filament was aligned axially and adjacent to the control grid or extraction electrode. This electrode had an aperture of 1.58mm and served both to control emission and to assist in beam focussing.

The einzel lens was asymmetric and consisted of three cylinders with the middle one of slightly smaller diameter and overlapped by the outer two. The first electrode of the lens had an aperture disc spot welded to it on the filament side. The aperture was the same diameter as that of the grid and was added in order to increase the field strength near the filament. The resulting stronger

field enhanced electron extraction from the cathode to the lens. The disc also confined the field more and, by reducing the field penetration into the cathode space, tended electrostatically to isolate or decouple the cathode and lens regions. The second electrode of the lens was made into a cylinder, because it was found that broadening the field of the electrode strengthened the focussing ability of the lens.

It should be noted, that what was maximized from the gun was collected electron current. Focus, in the sense that it is used here, refers to current maximization, not necessarily to a focal point or axis crossover on the part of the charged particles. Linearity shown in Fig. 1.

2.3. Ionizer

The volume wherein ionization took place was referred to as the ionization chamber and consisted of two end grids and, in effect, a four-sided, wire wound "grid" enclosure. The parallelepiped volume was 0.57 cc. The grids were made up of 25μ W-Re (3%) wire, and the enclosure consisted of a continuous wire wound in a complex multiple figure eight pattern. The objective of so intricate a design was to provide an electric field which was uniform and precise while allowing the chamber to be externally cleaned by

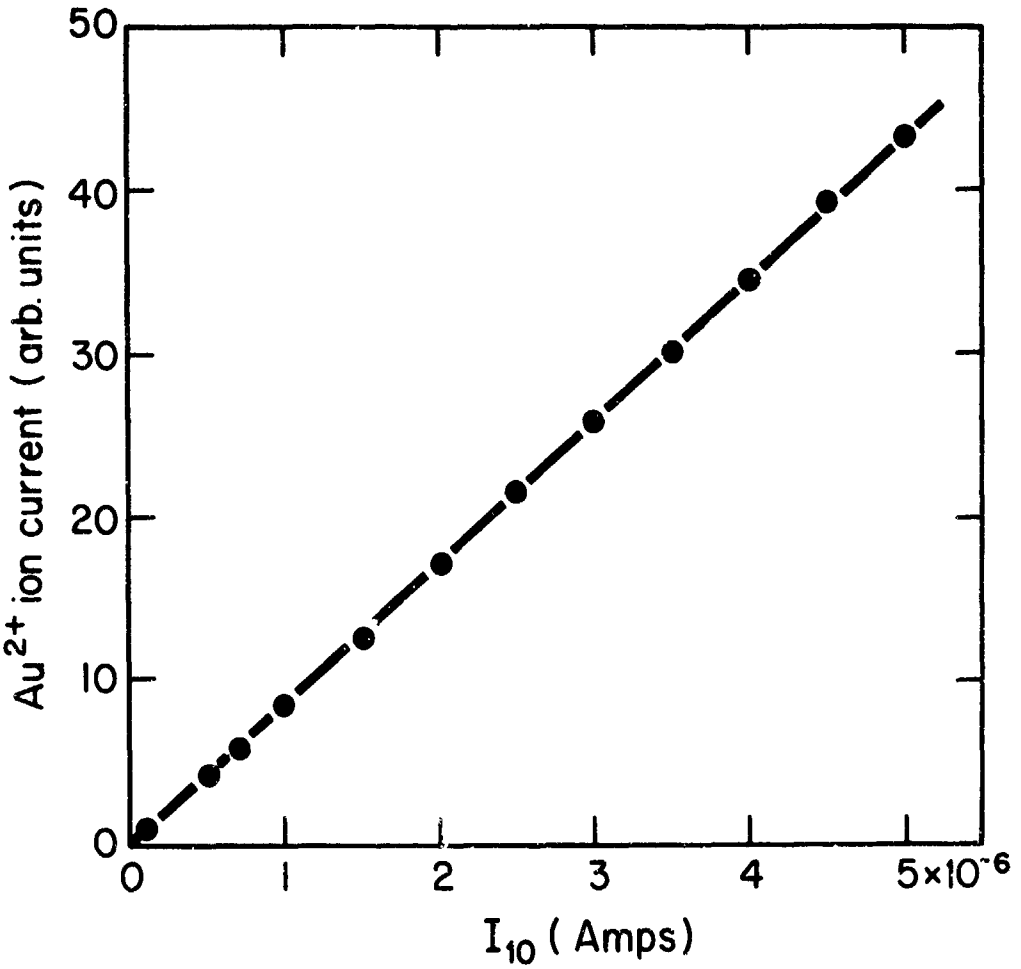

Figure 1: Linearity of gun output current with measured ion current. Au^{2+} was selected arbitrarily over other ion species.

flashing the grid wires with an electric current.[2]

In implementing the latter, care had to be exercised that the wires were never heated to the point where the tungsten and alumina insulators would react (~2000°K).

The ion draw out field V_{ID} was sustained by holding the ends of the chamber grid at different potentials. For V_{ID} = 12V. the steady state current flow I_{ID} = 68 mA., implying a steady state resistance of 166Ω.

Operation was maintained in the constant field extraction mode wherein each of the end grids was connected to the respective neighboring end of the chamber grid. Ions formed were directed either into the mass spectrometer or the ion collector, depending on the setting of a double-pole double throw selector switch.

The entire electron gun and ionization chamber were floated at V_{IE} above ground. This meant that the generated ions had a zero kinetic energy point approximately at potential V_{IE} - approximate because the ions need not be formed with zero initial velocity. Since the mass spectrometer entrance was at ground, V_{IE} also represented the acceleration potential and, thus, the approximate entering energy of ions. The ions traversed a two electrode lens at potentials V_{IF} and ground focussing them toward the mass spectrometer (or ion collector

where V_{ES} replaced V_{IF}).

The electrode configuration was such that a focus could be obtained at a positive and negative value of V_{IF} for each given V_{IE}, although the magnitude of the V_{IF} voltages was not the same. The focus for positive V_{IF} was much sharper than for negative and required about an order of magnitude lower potential. It should be noted that the term focus in this discussion refers to a maximization of spectrometer output and not necessarily to any kind of beam crossover point. The former is, of course, a more meaningful measure in the context of the experiment at hand.

If the system was set for ion collection there was no need for concern about focus, and the counterpart potential to V_{IF}, which was V_{ES} applied to electrode 5E, served a different purpose. With $V_{ES} = 0$, 5E was at ground, as was the ion collector and its entrance grid. The polarity was such that for $V_{ES} > 0$, 5E was biased below ground, such a field tending to repel electrons. The electron zero energy point was at $V_{IE} - V_{EA}$. The post acceleration electrons, which had an energy of V_{EA}, thus regarded the grounded collector as a potential barrier of V_{IE} and electrode 5E as V_{ES} more formidable than that.

It was essential to measure ion current caused by collision only and to screen out extraneous contributions of current arising from other sources. In order to prevent collection of electrons from the beam at the ion collector, the condition had to be satisfied that $V_{IE} > V_{EA} - V_{ES}$.

Furthermore, before coming under the influence of V_{IE}, the newly formed ions were subjected first to the small draw out potential V_{ID}. The most energetic of the ions impinged on the collector with approximate energy

$$E \doteq e\{V_o + (2/3)\ V_{ID} + V_{IE}\},$$

where $eV_o = 1/2\ mv_o^2$ and v_o is the initial ion velocity component in the direction of the collector. The 2/3 factor is an estimate of the periphery of the intersection area projected upon the length along which V_{ID} acts. e is the electronic charge carried by a singly charged ion. Because most of the atomic beam velocity was directed perpendicular to the collector direction, v_o was small. Empirically, so too was V_{ID} relative to V_{IE}. Note the larger component of initial ion velocity, perpendicular to the action of V_{ID}, has in effect, been considered. V_{ID} must be strong enough so that the parabollic path of the ion directs it through the chamber end grid before it reaches any of the side wall structure. This required

that the orthogonal component of velocity be small at the point of exit from the chamber.

Thus the ion impingment energy was approximately $V_{IE} \lesssim 200V$. This was too low to generate secondaries but could lead to the genesis of Auger electrons from the collector. In this regard, 5E at potential V_{ES} acted to prevent these electrons from leaving the collector. Because of this and its previously described function with regard to the beam electrons, 5E was called a suppressor grid.

As a final point, mention should be made of the great flexibility built into the entire ion optics system. The chamber, gun, and collector structures could be run in manners different from what is described here to investigate surface phenomena, Auger effects, focus behaviour, and to perform retardation experiments. The full versatility of the equipment was not developed in the course of this investigation, because the experiment was limited to cross section measurements. The adaptability of the design to other functions, however, is an asset not to be overlooked.

2.4 Electron Multiplier

The output of the mass spectrometer was fed into an electron multiplier in order to provide conversion and amplification of the ion signal. The multiplier was a Venetian dynode type with 22 dynodes and 21 stages of amplification. The lead dynode served to convert the incoming ion signal to an electron signal.[18]

Because the ions emerging from the spectrometer had wildly skewed trajectories, it was advisable to situate the multiplier as close as possible to the spectrometer output port. For the same reason dynodes with a large active area were used (2.5 cm square).

The requirement of proximity to the spectrometer drew the electron multiplier away from the support flange and similarly away from the anode and signal processing equipment. Initially, the distance was taken up by a direct wire transmission of the signal to the anode. This presented a noise problem, however, because of ringing that was induced by the high frequencies naturally present in the train of output pulses. In lieu of this, a drift space at the end of the multiplier was added. A slight focussing of the electrons was also present, as the resistances were divided unequally between the two electrodes.[27]

The dynodes were driven from one power supply divided through a chain of resistors. Metal guards were attached to every third dynode primarily to suppress field emission and secondarily to provide some shielding against random particle intrusion and false counts.

The electron multiplier was used as an ion counter connected in the so called amplifier-counter mode. It was expected that under normal operation, a saturation effect in counts/sec. could be observed as a function of applied voltage. This is a statement that the counting efficiency of the multiplier improves as the gain (applied voltage) increases. With greater gain more ions of lower energy or of lower incident angle - those ions producing a weaker response at the conversion dynode - become detectable. When all particles are detected, further increases in gain have no effect.

Such a saturation effect is shown in Figure 2. When quantitative results were required, the electron multiplier was operated at 4.6 kV. With time, the multiplier performance appeared to deteriorate and higher operating voltages were required. The figure gives data for an "older" multiplier. New dynodes generally displayed saturation in the range 3.5 - 4.0kV. The deterioration process was gradual, however, usually over a period of

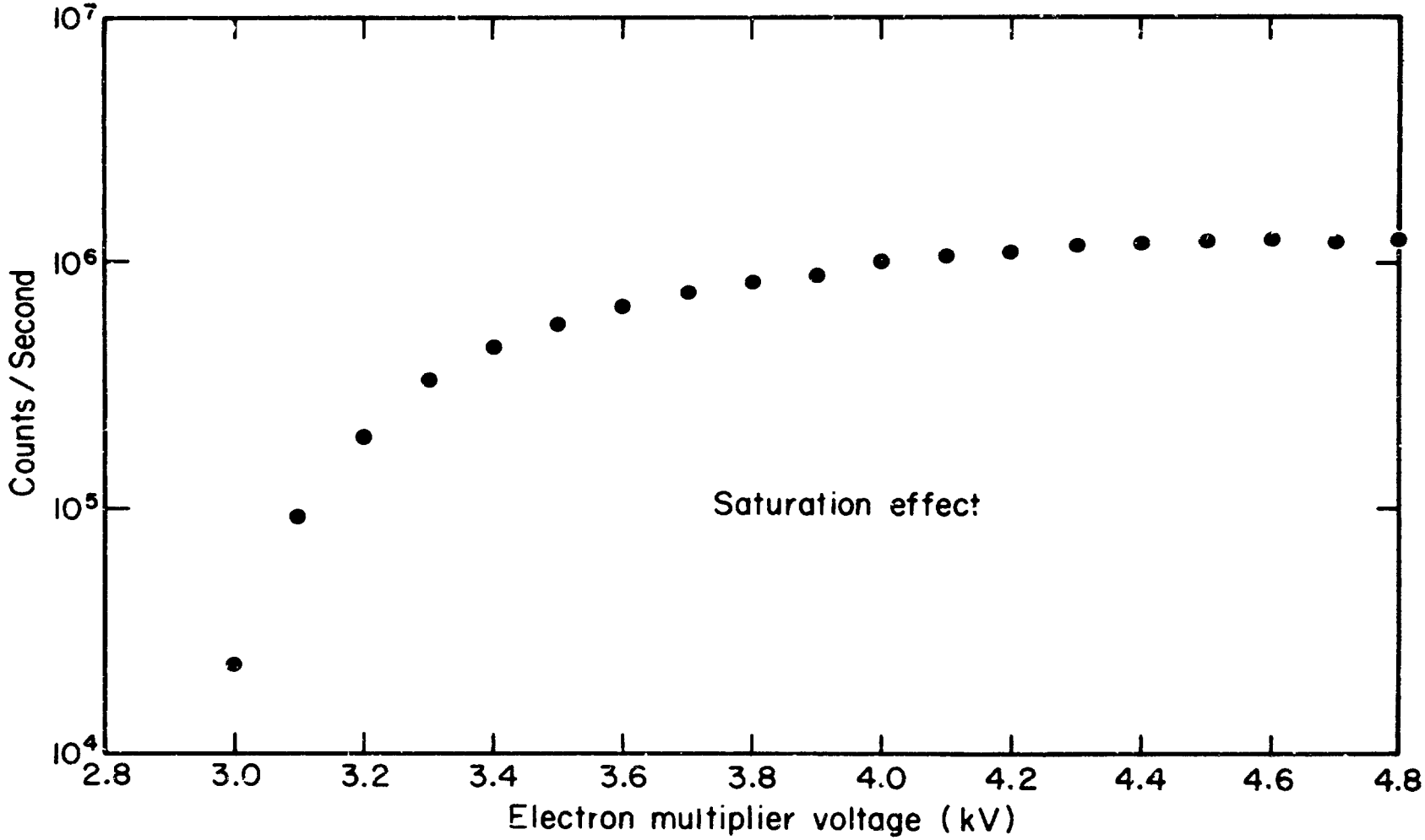

Figure 2: Saturation of detection signal with multiplier voltage.

several months, so meaningful data could be taken at any time so long as the saturation voltage was known.

Further and more pathological implications of the deteriorative process are discussed in a subsequent section.

2.5 Investigation and Procedure

In pragmatic terms, the major effort in the investigation was devoted to getting all sections of the apparatus to function correctly - at the same time. To this end, much of the equipment was rebuilt at one point or another, some with design modifications. This was necessitated either by out and out equipment failure or by the more common stability problems described in other sections of this report. The latter situation relates to a frequently observed condition wherein the sections of the apparatus functioned in an approximately correct manner, but outside the tight precision limits required for the experiment. In fact, it was usually the case at any given moment that all the equipment operated satisfactorily, except for one or two sections which were unstable or otherwise malfunctioning.

The investigation was further complicated and delayed by the necessity of moving the entire experiment, including all instrumentation, vacuum envelope and support facilities, to another location. The move took place in early June, 1973.

The experimental procedure reflected the natural separation of relative and absolute descriptions of the cross section data. The relative data was taken first on all species of a given element, then the absolute measurements were added.

Prior to any measurements being made, the system was generally left on for about an hour to assure that all thermal drifts and effects had ample time to equilibriate. A check was then made on some convenient background substance such as H_2O^+ or N_2^+ to test for stability and repeatability. This was done in order to preserve the element under scrutiny, since only a relatively small sample of the material could be put in the Knudsen cell for each experimental run.

When the system check out was completed, the power to the atomic source was raised until a satisfactory atomic beam was generated. Although the system output signal could theoretically be taken either at the output port of the pulse processing electronics or directly off the multiplier anode, the former was almost always used. In this regard, there could be no introduction of systemic error between relative and absolute measurement.

The signal was recorded simultaneously on an analog x-y recorder and digital voltmeter-printer assembly print out. The recorder provided a visual check on the gross features of the data. The digital presentation was more precise.

The objective was to determine the cross section as a function of electron bombardment energy. The procedure followed was to sweep the accelerating voltage V_{EA} of the electron gun in step-wise fashion. This was done either by hand or by a step function generator programmed into the V_{EA} power supply. At each step of a few volts magnitude, the specie ion current was recorded. The recording was delayed several seconds with respect to the stepping in order to allow the capacitive filtering action on the output signal to reach equilibrium. This was the reason for a discrete rather than a continuous sweep mode.

This procedure was followed over the entire voltage spectrum under two conditions - with the atom beam shutter open, and with it closed. Thus it was possible to determine separately, all other parameters constant, the output ion current for signal plus background and for background alone. A direct subtraction of the two then lead to the signal ion current. Since the cross section is directly proportional to the ion current, the constant of proportionality was the only remaining requirement neces-

sary for an absolute determination of the cross section value.

In order to prevent the introduction of systemic or repetitive procedural errors, the voltage scans were taken in both directions both for the background and for the signal components. In light of the hysteresis problem described subsequently, the bi-direction scanning provided one necessary check on data repeatability.

Because the signal amplitude was not stationary in time, also discussed later, a quick succession of data points was taken at the extremes and middle of the voltage spectrum after each scan. This was done as an adjustment of the relative position of the cross section points and eliminated any temporal dependence of the output.

Finally, a straight arithmetic average was taken over numerous such runs for each ion specie, in order to establish the final relative configuration of data points.

Having determined the intra-specie relative cross sections, the next step was to measure the inter-specie relative amplitudes for each element.

Since an entire curve of relative data is absolutized by fixing any point on that curve absolutely, this measurement had to be made at only one point. That point was chosen for convenience for each element. In that choice, cognizance was taken of the facts that the cross sections for higher orders of ionization peak at correspondingly higher electron voltages and that one loses approximately an order of magnitude in cross section amplitude with each successive ionization order.

The ratio of specie amplitudes was of necessity taken with the electron multiplier in saturation, usually ≥4.6kV, and with all pulse processing operations included.

At the completion of the relative data measurement, it was possible to write formally

$$\sigma = kI^{+} = \frac{KI_m^{+}}{NLI_e} = K\sigma_R$$

where I_m^{+} is the measured ion current for a given specie, σ_R is the measured relative ionization cross section, and K is an unknown constant of proportionality.

In order to determine the actual value of σ, it

is first necessary either to evaluate K for the relative data or to make another experimental measurement at one data point with K = 1. The latter approach was the one used and required measurement of the total ion current signal. To accomplish this, the generated ions were collected instead of being swept into the mass spectrometer. Totality was checked by observing a saturation of total ion current, I_{12}, with increasing V_{ES}.

The atom beam itself was collected on a quartz crystal which served as a transducer for a film thickness monitor. Consistency was checked by observing that the monitor reading did not change when the shutter was closed. The rate of deposition was measured over a given time period at the experimental conditions.

The atom gas temperature in the Knudsen cell, which was also necessary to determine the average particle velocity and neutral density, was not measured directly. It was estimated from thermodynamic considerations. This and other calculations that have to do with this section are presented elsewhere.

3.0 STABILITY CONSIDERATIONS

3.1 Internal Problems

Much of the time spent during this investigation was passed in trying to remedy various stability problems that arose during the course of the experiment. Some of the more serious problems are described separately in other sections. In addition to these, however, there were numerous instabilities of a less spectacular nature that had to be individually isolated and resolved before reliable, coherent output could be obtained. Because it was common to deal with measured ion currents of $\sim 10^{-12}$ A, as well as with electron gun currents of 10^{-6} A., even small irregularities could reflect through the system and cause disturbances.

A floating support electrode in the atom source filament assembly was the cause of one subtle stability problem. The heated filament apparently shifted position slightly during operation so as to barely relinquish contact with the support electrode. As the electrode was isolated electrically and very nearly touching the filament, there ensued a sequence of negative charge build ups and micro-discharges between electrode and filament.

The arcing current was transmitted through the sys-

tem via the internal circuitry and manifested itself as small spiking in the gun elec rometer. The support electrode was subsequently connected through a 1KΩ resistor to one of the feed electrodes of the filament, and the symptoms disappeared.

Another stability problem arose in the feedback control function of the electron gun due to an overheated, and hence noisy, damping resistor. The role of the resistor was to limit and absorb oscillations associated with feedback, and the noise difficulty was easily resolved by replacing the resistor with one of greater thermal capacity.

The mass spectrometer also contributed to this kind of problem on several occasions. Some of the vacuum tubes deteriorated with age and had to be replaced. A loose coil connection in the tank circuit and a faulty relay-operated switch, at different times, caused the spectrometer output to be unsteady.

In the signal processing portion of the equipment, one of the wide-band amplifiers steadi y declined in performance over the course of the experimentation, requiring eventual replacement. Also, the low pass filter used for data recording purposes to sift out the rapid oscillation which emerged at the output of the ratemeter

was redesigned and rebuilt. The new filter was an improvement not only in stability but also in capability, as it contained a solid state operational amplifier instead of a tube type amplifier which had been used.

The list could be continued, but the preceding gives an indication of some of the typical stability problems that were continually encountered in trying to get reliable, repeatable data. In general, the difficulties ran the gamut from marginal mechanical contacts hidden deep within instrumental and physical circuitry, to electrode and insulation problems within the vacuum envelope.

The subtlety of some of the problems was enhanced by involvement with such factors as thermal effects and intermittency. Thus sometimes the instabilities would appear after some period of operation and sometimes not at all. Furthermore, there was frequently more than one cause compounding the issue. Suffice it to say, the equipment was not completely "de-bugged" from a production engineer's standpoint and required constant and sophisticated maintenance.

3.2 Hysteresis

One of the recurrent systemic problems associated with the electron gun resulted in hysteresis-like behavior. The relative output, in terms of cross-section measurement, displaying the hysteresis is presented in Fig. 3. Behaviour related to the same phenomenon, although not strictly hysteretic, is shown in Figure 4.

The cause of this kind of erratic performance was found to be a buildup of a contamination layer on some of the electrodes and conducting surfaces within the gun structure. Such contamination was itself non-conducting and behaved like an insulator. The presence of charged particles in the region led to a build-up of charge on the non-conducting portions of the electrodes. This distorted the electric field configuration which, in turn, altered the trajectories of the electrons.

Monolayer formation under these conditions may be discussed by considering the intensity of bombardment of a stationary surface by molecules from a gas. If that gas is, as a whole, not

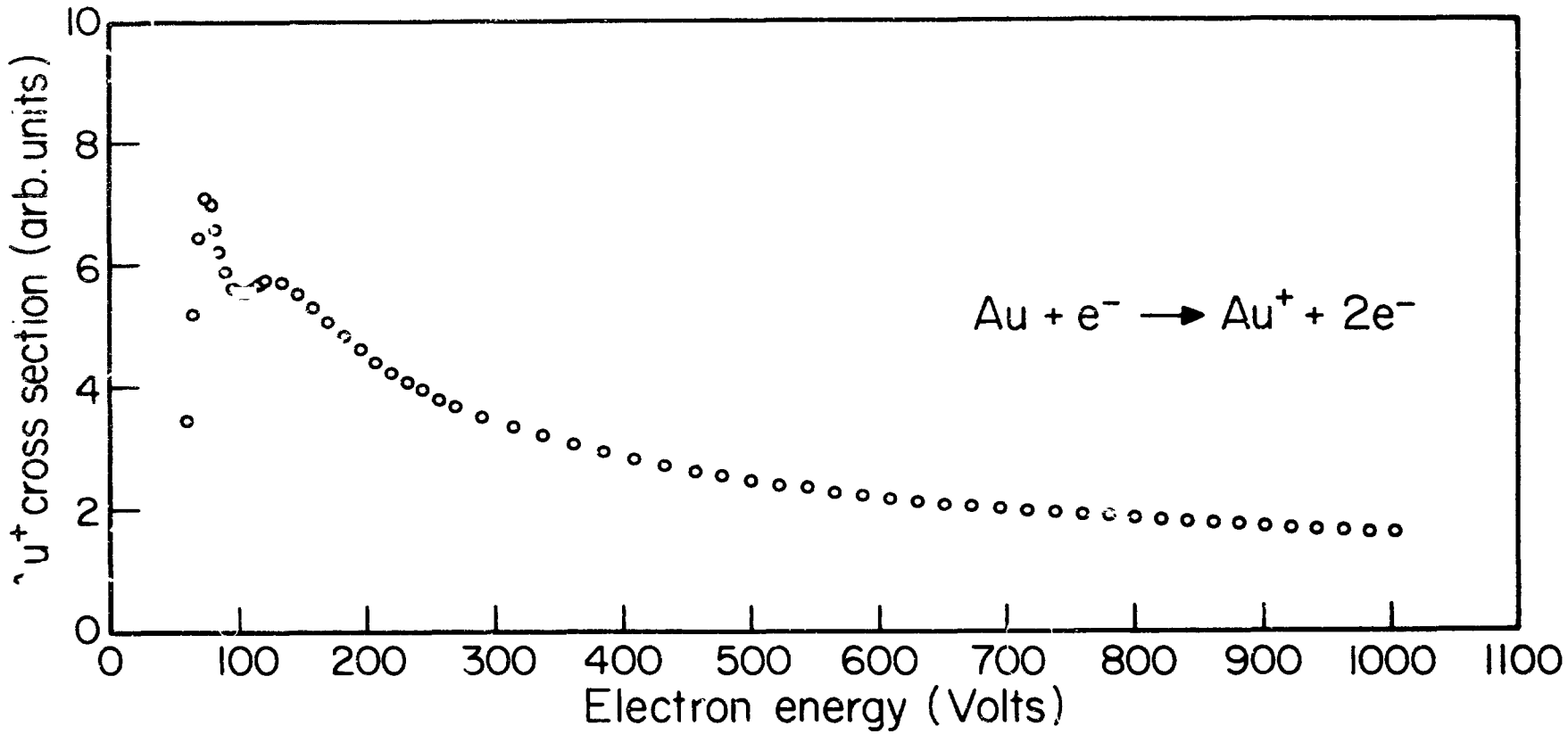

Figure 3: Hysteresis effect on Au^+. The data were taken from low to high energy. The dip at 100v. is spurious and did not occur in the same manner when the direction of energy traversal was reversed. It also did not occur after the contamination problem was resolved.

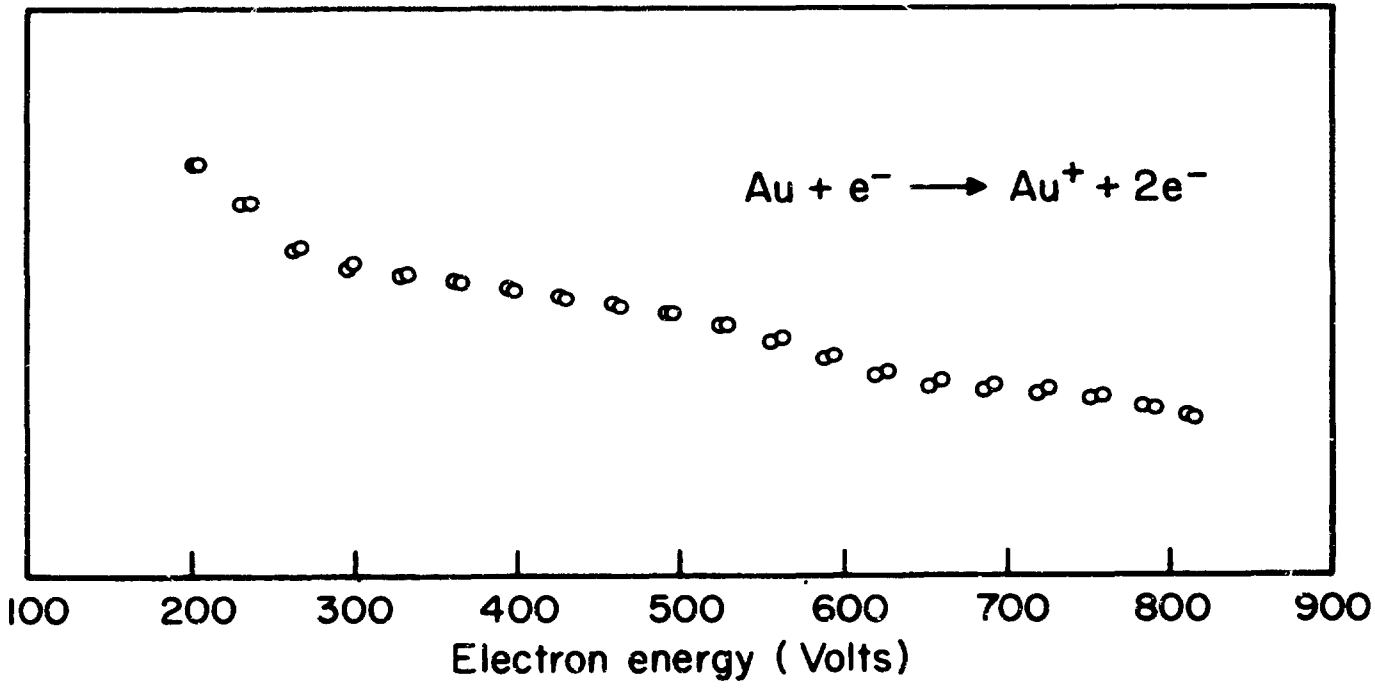

Figure 4: Unusual example of relative cross section data afflicted with "hysteresis" yet repeatable. The two runs were taken back to back, both in the direction of increasing energy. Although ordinarily not repeatable, occasional instances such as this tended to obfuscate the diagnosis and treatment of the problem. Ordinate axis units are irrelevant.

moving with respect to the surface, the number of molecular impacts per unit time and unit area is

$$\nu = 1/4n\bar{v} \quad \#/cm^2/sec.$$

where n is the number of molecules per unit volume and $\bar{v}$ is their average velocity. Under the assumption of a Maxwell-Boltzmann distribution

$$\bar{v} = (8kT/\pi m)^{\frac{1}{2}} \quad cm/sec.$$

so that at $T \approx 300^{o}K$, $\bar{v} \approx 45 \times 10^{3}$ cm/sec.

Not all impacting molecules undergo adsorption, so one must introduce a sticking probability coefficient s. The number of molecules adhering to the surface is then

$$\nu_s = \frac{s}{4}n\bar{v} \quad \#/cm^2/sec.$$

The length of time τ it takes to deposit a monolayer on a surface is

$$\tau = \frac{N}{\nu} \quad sec.$$

where N is the number of molecules/cm^2 in a monolayer. Recalling P = nkT, the monolayer formation time becomes

$$\tau = \frac{N(2\pi mkT)^{\frac{1}{2}}}{sP} \text{ sec.}$$

A monolayer is generally considered formed when approximately ¼ of the surface is covered with adsorbed gas. This implies $N \simeq 2.5 \times 10^{14}$ at./cm.^{2} At $P = 10^{-8}$ Torr and $s = 0.5$, $\tau \simeq 100$ sec.

It was found that subsequent to disassembly, thorough cleaning and replacement of the electron gun, the hysteresis behaviour did not return until after about 20 minutes of operation had elapsed. The length of this time period suggested that the contamination problem was not simply a matter of monolayer or multilayer formation from thermodynamic origins. Rather, it was more likely a complex set of chemical reactions at the metal surfaces, involving some of the organic derivatives of the pump system and induced by the energy transfer from electron bombardment. Superficial inspection of the contaminated areas revealed both the carbonations nature of the deposit and the erstwhile presence of local heating.

The term hysteresis is used here to denote that different outputs were obtained depending on whether one proceeded from low electron energy upward or from high energy downward. It is not to be assumed that

the plots themselves were necessarily repeatable. In fact, the unstable nature of the contamination effect ordinarily precluded repeatability even if the same energy direction was taken. Figure 4 provides a counter-example.

Note also that the discrepancy between "up" and "down" was manifest in the intermediate energy range. At the high and low ends, the data were in agreement. At high energies, presumably, this was due to the fact that the fast electrons were undeflected by the relatively weak perturbation field set up near the contaminated electrode. Also there may well have been some removal of the deposit by high energy electron bombardment.

Moreover, the form of the cross section versus electron energy curve is such that as the energy increases above the peak the slope decreases markedly - approaching zero. At high energy, therefore, variations in electron velocity will have a much less pronounced effect on the cross section, and hysteresis will be much less noticeable even if the effect is present.

At low energies, it is possible to speculate that the deflection imposed on the transiting electrons

is reduced. The low velocity does not allow for close approach between the repelling bodies. Furthermore, one would expect fewer electrons would reach the insulating layer to build up the perturbing charge. This would enhance a diminution of the repulsive forces.

This is, in a sense, analogous to a cross section discussion where the likelihood of collision reaches a maximum at some intermediate energy. The contamination effect is indeed, similar to a cross section problem in that the involvement has to do with electrostatic forces between electrons, some of which are moving. The energy dependence is thus not unexpected and would be anticipated to be not radically different in form from the ionization cross section data.

Again it must be emphasized that there was considerable variability in terms of contaminant induced effects. The energy band where hysteresis obtained was not precisely defined and even occurred on occasion at the energy limits. In general, however, the foregoing description was typical if not binding. It was not part of this investigation to study the

contamination hysteresis in depth, so no data were taken to quantify the parameters governing the phenomenon. Rather attempts were made to find ways to get meaningful experimental results in spite of the presense of this perturbing effect.

3.3 Electron Multiplier Instability

A particularly troublesome instability manifested itself as a significant random shift in output signal. The recurrent changes in level appeared to be unrelated to any electrical or physical input parameter and were of indefinite duration as well as intermittent.

Figs. 5 and 6 present a graphic display of how the unstable signal was reported by the system. Fig. 5 shows a sample set of Au^+ cross section data afflicted with this instability. The electron energy at which the level change occured was not a significant factor in that it was not repeatable. Fig. 6 displays typical output signal levels taken at constant energy for N_2^+. The temporary stability at different levels for constant conditions was typical.

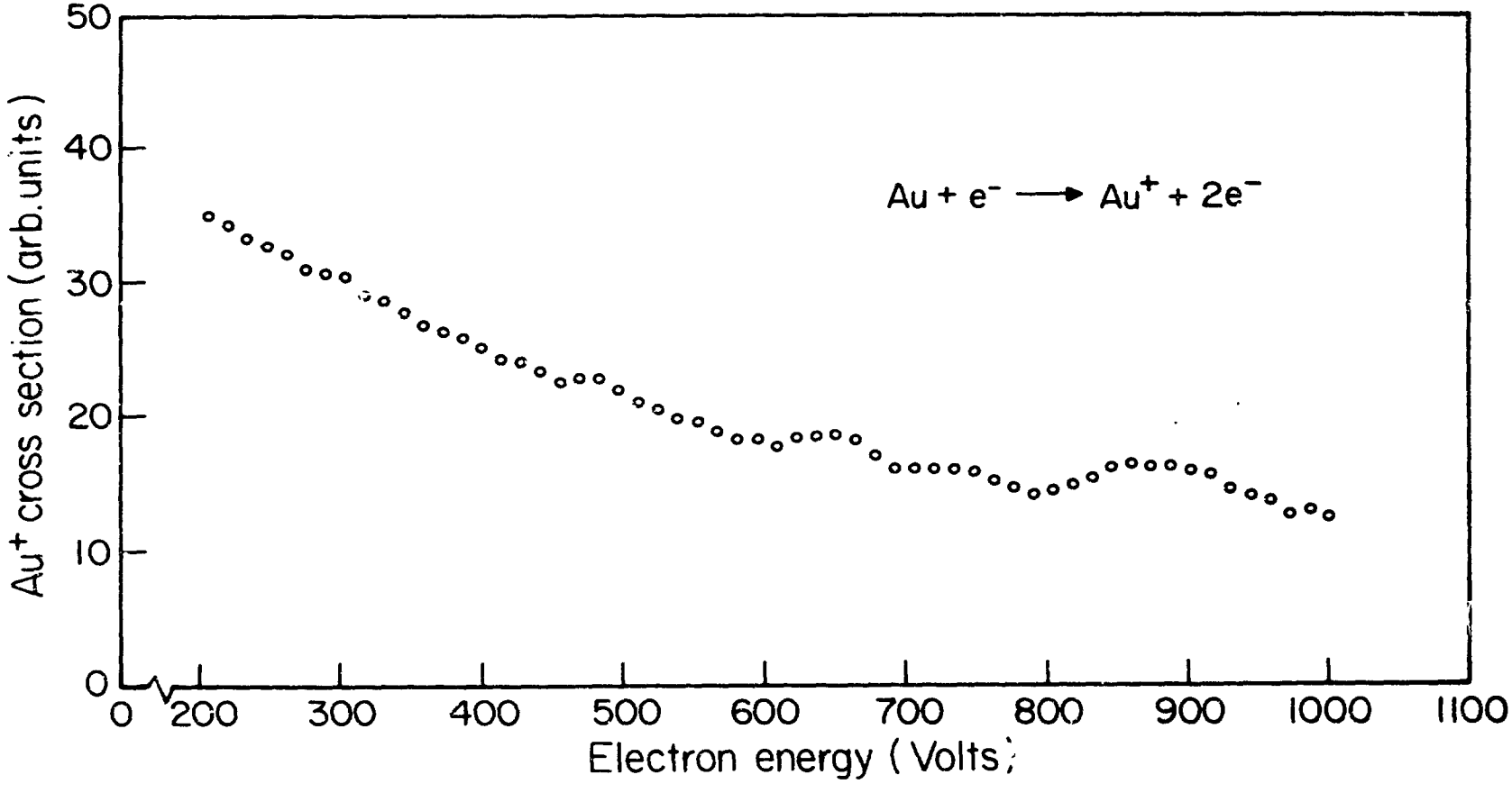

Figure 5: Au^+ cross section data - unstable due to electron multiplier problem.

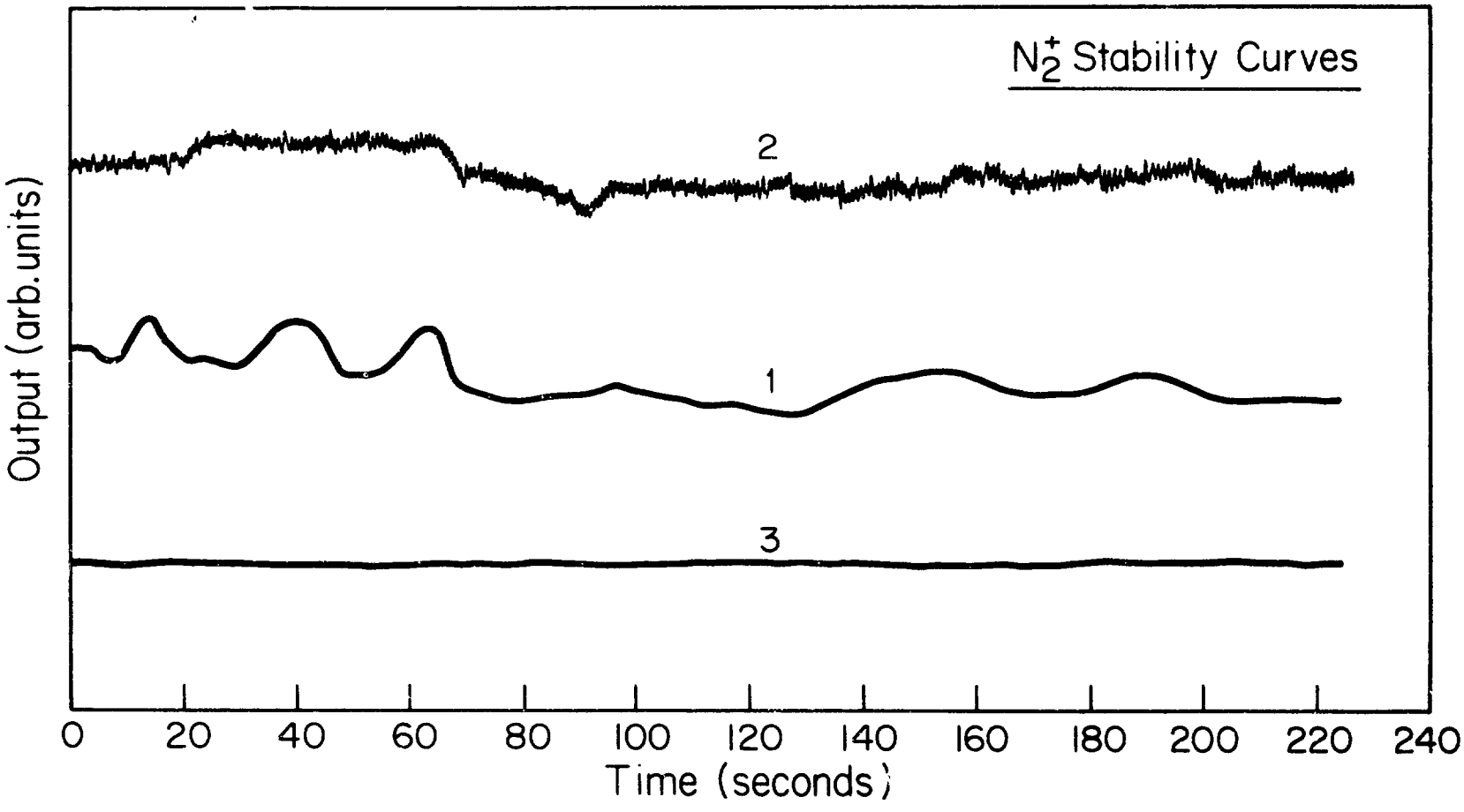

Figure 6. N_2^+ cross section data taken at V_{FA} = 100V. and plotted as a function of time. (1) Output of full system. (2) Output excluding low-pass filter. (3) Output of full system after resolution of electron multiplier instability. For (1) and (2) the largest fluctuations amounted to about 20-25% of the signal. For (3) the stability was good to better than 1%.

The possibility that the culprit was some kind of field phenomenon or incidence of stray particles led to a rebuilding of the multiplier with the shield geometry redesigned. It was thought that although such a redesign might not cure the problem, it would at least alter the electrical conditions so as to induce a change in characteristics. No such change was observed.

A series of bakeouts was performed to try to eliminate any contamination that might have built up, causing unstable resistive paths somewhere in the multiplier structure. The most demanding of these bakeouts required an eight hour heating at 400° C. The length of the heating cycle was determined by the tortuous thermal conduction path of the multiplier structure vacuum. Higher temperatures were precluded by the glass-enclosed resistors in the divider chain. As it was, some of the glass resistor casings "bubbled" due to too high temperatures. No change in the fluctuations resulted.

Instabilities in microwave beam tubes, such as klystrons, have been observed that are somewhat

reminiscent of the behavior here. In klystrons there is a phenomenon known as "skipping" which is an irregular shifting of the operating frequency of the tube off the design frequency and back. That problem was identified as being due to secondary electrons originating at the collector and drifting back into the output cavity region of the klystron. The solution was to bias the collector sufficiently off ground so as to trap any secondaries within the collector volume.

The particular electron multiplier in this experiment had a special drift space and collector appended to the dynode amplifier structure. Suspicions were thus aroused that some particle or electrical interaction in the collector region was interfering with the multiplied electron beam and causing fluctuations. Accordingly, the collector bias was first increased and then decreased in order to cause some change in the character of the instability. No such change was observed.

Technical notes from the manufacturer (EMI)[28] suggest that the dynodes may be left in dry air for up to 24 hours without loss in gain. No mention of a

possible stability problem is made, nor, apparently, has it been observed. Private communication with EMI failed to identify the fluctuations as recognizable dynode deteriorative behavior.

When the system was vented, it was always done with dry nitrogen to avoid any introduction of moisture onto the dynode surfaces. Although there were periods in excess of one day when the dynodes were at atmospheric pressure in the dry nitrogen, at no time did the multiplier come into contact with moist air.

The activation procedures for deteriorated dynodes were considered. The first was recommended by EMI, if the multiplier gain fell after repeated exposure to air. It consisted of filling the vacuum envelope with oxygen at a pressure of about 10 Torr. Then with the middle dynode (number 11) grounded, a 1MHz, 2.5kV signal was to be introduced at the first dynode. The voltage was subsequently to be adjusted such that there was a 0.5 mA. discharge current maintained. This condition was to be sustained for about one minute. After this, the same signal was to be applied to dynode 22 (dynode 11 still at ground), and

the same procedure followed.[28]

A cursory glance at the requirements just described indicates that what was called for was virtually a radio transmitter with the concomitant problems of shielding, etc. After a few attempts to come up with a realistic way of implementing this activation method, it was finally discounted as impractical.

The second procedure was an in-house technique which had been developed by technicians at M.I.T. and had been applied with some success to similar dynode configurations. It consisted of immersing the dynode chain in an evacuated chamber ($p \sim 10^{-5}$ or 10^{-6} Torr) and individually rf bombing each of the dynodes successively. Each dynode was brought just up to color ($T \approx 800^{o}C$), and held there until the system recovered the original pressure. After all dynodes had been treated thusly, the chamber was back flushed with dry He and the dynodes bagged in a He atmosphere, so there was no exposure to air.

This approach suffered from the disadvantage that the multiplier in this case had to be completely disassembled, since the resistors could not withstand

in excess of 400°C. Once disassembly became necessary, however, it was just as easy and more reliable to replace the used dynodes with brand new ones than to gamble on activating the old ones.

As it turned out, the instability proved to be a dynode deterioration problem, although such behavior had not been observed elsewhere. With new dynodes, the fluctuations disappeared. In the final stages of the investigation, the electron multiplier was kept under vacuum as much as possible. When venting was necessary, the non-vacuum time was kept to a one hour maximum, and then always in a dry nitrogen atmosphere. This procedure lengthened the lifetime of a set of dynodes from about three to about six months or more.

It should be noted that the objective of this experiment was to obtain cross sections, not to study the characteristics of BeCuO dynodes. Thus, much of the nature of this phenomenon remains unexplained. Whether the performance decline was, for example, a contamination problem or a surface deterioration effect, and why the symptoms manifested themselves

as this particular instability, are simply not known at this time.

It was observed, however, that along with the fluctuations, the older dynodes exhibited a somewhat reduced gain compared to a new, unused dynode set.

Gain for the electron multiplier was roughly estimable by the following technique. With the multiplier on, cosmic rays and stray phenomena would induce occasional output pulses visible on an oscilloscope. An ordinary pulse appeared as a spike with a capacitive decay and could be described as

$$V(t) = V_o e^{-t/\tau}$$

and

$$\frac{dV(0)}{dt} = \frac{V_o}{\tau}$$

where V_o is the initial pulse height, and τ is the time constant.

Thus, τ can be read off the oscilloscope by extrapolating the slope of the decay portion of the pulse to the baseline or time axis.

Now

$$\tau = RC,$$

and for a standard oscilloscope R = 1MΩ, so

$$C = \tau \times 10^{-6} f.$$

For any capacitance Q = CV. At t = 0, Q = CV_o, so Q is known. Under the assumption of an initial electron causing the event, it follows that the gain is approximately

$$G = \frac{Q}{q_e} = \frac{V_o \tau \times 10^{-6}}{q_e}$$

Note this is the gain of the multiplier allowing for the first dynode to be a conversion dynode, and under the restriction that only one electron results from the conversion process. Also the pulse chosen for analysis must be "typical" in amplitude and shape.

4.0 ELEMENTS INVESTIGATED

4.1 Gold

Gold wets the common refractory metals, W or Mo, which might be used as Knudsen cells in the atom source. This obligates some care in design, since if the molten gold reaches the collimator some of the gold will be lost. In liquid form the gold can flow up through the small holes in the collimator or out along the boundary between collimator and cell. In addition to losing part of the charge, the errant gold can cause a short circuit between filament and cell and/or solidify in an awkward location within the atom source structure.

The most mechanically convenient of the refractory metals, tantalum, is completely precluded from use with gold because the two elements react at moderately high temperatures. The reaction produces an interesting alloy, but concommitantly destroys all structural integrity of the tantalum parts at temperatures far below the melting point of pure tantalum. Such effects were observed first hand during the course of this investigation. In light of this the Knudsen cell and collimator were constructed from molybdenum. The gold charge was simply kept small enough so that there was no flowing on the melted surface when the gold was molten. Data on Au^{+}, Au^{2+}, Au^{3+} were generated.

The output ion beam characteristically displayed a slight gradual decline in amplitude with time. The decline was due to a reduction in the intensity of the atomic beam emerging from the Knudsen cell, which in turn, was due to a lowering in the temperature of the charge as it evaporated. The falling temperature was a result of small thermal conduction losses from the bottom of the cell through the physical support and electrical connection network.

The thermal sink and gradient effect was not unique to Au and was similarly present during the investigations on Fe and Cr.

4.2 Chromium

Chromium presented no problem in terms of chemistry in that it was stable with the refractory metals and with carbon. A cell of carbon was used with a collimator of molybdenum with no adverse effects. The Mo collimator was chosen simply for convenience.

There was some difficulty, however in generating an atomic beam of Cr because of the evaporation characteristics of the metal. The vapor pressure of Cr for a given temperature is only slightly lower than that

of Au (1063°C). This is one manifestation of the fact that Cr sublimes.

In terms of the experiment, this meant that the required vapor pressure for a Cr beam could be achieved at a temperature well below the melting point. The difficulty arose because the Cr pellet did not melt and, therefore, did not flow.

Consider a pellet of Cr in the Knudsen cell. There is a solid contact between pellet and cell at the bottom and partial contact along the sides. The top of the pellet is subjected to radiational cooling and the bottom to cooling by conduction through the base of the cell. Heat enters, in the main, by conduction from the side walls of the cell through the side wall of the cylinder. A temperature description of the Cr under operating conditions would thus show isotherms bowed toward the center of the cylinder. The hottest area would be at the periphery of any radial plane and toward the middle of the pellet along the z-axis.

In terms of the mechanics of evaporation, because the cylinder sides are not in complete area contact and because of the radiational cooling at the top, one would expect that more intense evaporation would come from the

sides and as one proceeds toward the mid-length of the evaporant. After partial evaporation, then, the Cr would maintain its cylindrical symmetry but the radius should decrease as one approaches the mid-height of the pellet. In other words, the cylinder should appear to have an axial surface that is concave inward. Such an effect was indeed observed during the investigation by removal and inspection of the Cr pellet after some of it had been vaporized in the atom beam source.

Once this configuration began to develop, however, there was a problem with the Cr pellet as evaporant structure. Since the side wall of the pellet was not only the hottest surface, but also the conduit for heat entering from the Knudsen cell, as that wall evaporated the conductive path between cell and pellet disappeared. This changed the thermal configuration in the Knudsen cell and also altered the scheme of heat entry and loss, placing much greater emphasis on radiation as a transfer mechanism. The new situation required considerably higher power from the electron bombardment energy source. With the higher power the signal to noise ratio for Cr^+ at V_{EA} = 200v. was ~11:1 and for Cr^{2+} was ~36:1.

In essense, the preceding analysis explains two effects which, from the experimentalist's perspective

initially appeared pathological. The first was a rather immediate and rapid fall in Cr ion output signal with all parameters holding constant. The second was a consistently weak signal in reference to what had been obtained for Au and in light of the known pressure-temperature data for Cr.

Presumably some improvement in power efficiency could have been secured by using Cr in powder or chip form where conduction might have been maintained. Additionally, the literature suggests electrodeposition of Cr on refractory filaments as an appropriate evaporation technique. These approaches were not explored.

Cr is the only element of three investigated for which the triply charged ion is not presented. The atomic weight of Cr is 52, the mass to charge ratio for Cr^{3+} is 17.3 using electron units. The m/q ratio for H_2O^+, however, is 18 and that for OH^- is 17.

Since water was one of the major background contaminants and Cr^{3+} was a relatively small component, the signal was virtually inundated by the background noise, and all but undetectable.

4.3 Iron

Reference to phase diagram literature reveals the well-known fact that iron enters into solution with the refractory metals if the amount of iron exceeds 30% by weight of the metal sample. This phenomenon precludes a crucible-type structure where the crucible is a refractory element. The restriction on the amount of iron which can be used as charge in such a situation makes practical atom beam genesis impossible.[36]

To get around this, initially, a carbon Knudsen cell was designed with a collimator similarly of carbon. Apparently, however, iron also has a high temperature reaction with carbon which, to the misfortune of this construction, led to the rapid destruction of the entire cell structure.

A Knudsen cell design which proved successful in generating an Fe atom beam consisted of a crucible of Al_2O_3 jacketed with a thin covering of Ta made from Ta sheet stock. The cell was connected electrically by a Ta wire spot welded to the base of the jacket. No collimator was used but rather a cap with a small orifice.

An interesting focussing effect of the electron

bombardment structure was revealed in that after operation, inspection of the cell revealed a hole burned in both the Ta and the Al_2O_3. This effect was definitely repeatable. The location of the hole was between the two filament electrodes in the region of the 1/4 turn overlap of the "spiral" filament.

That such focussing action was not observed with the other elements was probably due to the more massive character of the standard (refractory) crucibles. The greater wall thickness and conductive capacity distributed the heat through the cell before one area became destructively hot.

An attempt was made to prevent the focus-induced puncture of the cell. A small hole was drilled in the Ta jacket about the size and at the location of the focus spot. Then a thin layer of conducting material was deposited on the exposed surface of the Al_2O_3 crucible, care being taken not to have the conducting deposit extend beyond the perimeter of the hole and make contact with the Ta jacket. In practice this was accomplished by scraping the Al_2O_3 with a Ta wire. The hardness of the alumina caused the Ta to scrape off and leave a deposit on the crucible surface.

The idea behind this construction was that the

conducting patch on the alumina was electrically isolated. In the presence of electron bombardment it would charge up negatively to a sufficient voltage so as to limit the impingment of electrons on the Al_2O_3 at that spot. It was found that there was a significant improvement in cell longevity with the "defocussi" construction.

Fe was the highest temperature element, in the vapor pressure sense, that was investigated. With the above design a strong enough atomic beam was generated to obtain data on Fe^+, Fe^{2+}, Fe^{3+}.

5.0 ANALYSIS AND DATA

5.1 Experimental Calculations

The Knudsen cell atom source is an approximation to an ideal effusion source. Under the assumptions of an ideal emitter and with the condition that the Maxwellian distribution of atomic velocities is maintained, it is possible to derive an expression for the number of atoms N effusing into an element of solid angle $d\omega$ per unit time.[21,32]

$$N(\theta)\, d\omega = \frac{n_s \bar{v}_s A_s}{4\pi} \cos\theta\, d\omega \qquad \text{atoms/sec.}$$

where θ is the angle of observation relative to the normal to the aperture. The area of the aperture is A_s. n_s is the number of atoms per unit volume in the cell and $\bar{v}_s$ is the average velocity of these atoms.

By kinetic theory,

$$\bar{v}_s = (8kT_s/\pi m)^{\frac{1}{2}} \qquad \text{cm/sec}$$

where m is the atomic mass and T_s is the absolute source temperature; and $P_s = n_s k T_s$. Some care must be exercised in handling the equations in order to assure consistency of units. k is particularly susceptible to different

interpretations depending on the derivation. Thus $\bar{v}_s$, derived from energy considerations, leads to k in units of dyne-cm/^{o}K. The equivalent pressure unit is dyne/cm^2. In this experiment, pressure was more conveniently measured in Torr, whence

$$n_s = (9.66)(10^{18}) \frac{P_s}{T_s} \qquad \text{atoms/cm}^3$$

The number of particles leaving the cell is obtained by direct integration over θ

$$N_s = \frac{n_s \bar{v}_s A_s}{4} \quad . \qquad \text{atoms/sec}$$

Substitution yields

$$N = (3.51)(10^{22}) \frac{P_s A_s}{(MT_s)^{\frac{1}{2}}} \qquad \text{atoms/sec}$$

where M is the molecular weight (amu) of the evaporant. The directionality of the experimental source was observed to be axial within 0.1%. Thus, concern can be limited to considerations of intensity solely along the z-axis ($\Theta = 0$). The intensity Y varies inversely

as the distance squared, for the ordinary cosine law variation.

$$Y(0) = \frac{n_s \bar{v}_s A_s}{4\pi z^2} = \frac{N}{\pi z^2}$$

$$= (1.115)(10^{22}) \frac{A_s P_s}{(MT_s)^{\frac{1}{2}} z^2} \qquad \text{atoms/cm}^2\text{/sec}$$

At the point along the z-axis where ionizations occurs, z_i,

$$Y_i(0) = (1.115)\ (10^{22})\ \frac{P_s A_s}{(MT_s)^{\frac{1}{2}} z_i^2} \qquad \text{atoms/cm}^2\text{/sec.}$$

What is necessary for the cross section calculation, however, is not intensity but neutral density. Physically, the intensity is the number of particles impinging on a square centimeter of area per unit time. This is representable as the number of particles per unit volume times their speed (on average) along the normal to that area.

$$Y(0) = n\bar{v}_a \qquad \text{atoms/cm}^2\text{/sec}$$

Because the beam is practically confined to a very narrow spread about the z-axis, it follows that stringent restrictions are placed on the lateral velocity components x, y. In particular, $\dot{y}^2 << \dot{z}^2$, $\dot{x}^2 << \dot{z}^2$, and therefore, the former are negligible in the exponent of the above elemental distribution function. Furthermore, the beam confinement condition requires

$$(\dot{x}^2 + \dot{y}^2) \leq \dot{z} \tan \theta_h$$

where θ_h is the small half angle of the beam cone. This leads to the largest value of $\dot{x}$ or $\dot{y}$ being

$$\delta = z \tan \theta_h$$

Application of these conditions and integration yields

$$\bar{\dot{z}} = 3/4(\pi)^{\frac{1}{2}} (2kT/m)^{\frac{1}{2}}$$

$$\bar{v}_a = (9\pi kT/8m)^{\frac{1}{2}} \qquad \text{cm/sec}$$

At the point of ionization in the ionizer, the neutral density is

$$n_i = \frac{Y_i(0)}{\bar{v}_a} = (6.56)(10^{17})\frac{P_s A_s}{T_s z_i^2} \qquad \text{atoms/cm}^3$$

where $\bar{v}_a$ is the average velocity of the atoms in the beam and is assumed to remain constant over the traversal path.

The Knudsen cell establishes a virtual equilibrium between phases of the element within the cell. This means the distribution of velocities in the atom gas in the cell is Maxwellian. For such gas the velocity distribution function can be used to determine the number of atoms per second crossing a unit area normal to the z-axis with velocities within the range $(\dot{x}, \dot{x} + d\dot{x}; \dot{y}, \dot{y} + d\dot{y}; \dot{z}, \dot{z} + d\dot{z})$. The result is

$$dN(\dot{x},\dot{y},\dot{z}) = (m/2\pi kT)^{\frac{1}{2}} \{n\dot{z} \exp\left(\frac{-m(\dot{x}+\dot{y}+\dot{z})}{2kT}\right) d\dot{x},d\dot{y},d\dot{z}\}$$

The average velocity along the z-axis is obtained through the usual method of integrating the weighted distribution on function and dividing by the integrated function. Thus,

$$\bar{\dot{z}} = \frac{\int_0^{\infty}\int_{-\delta}^{\delta}\int_{-\delta}^{\delta} \dot{z}\, dN}{\int_0^{\infty}\int_{-\delta}^{\delta}\int_{-\delta}^{\delta} dN} .$$

Beam Analysis

In the experiment, the atom beam was collected on a gold-coated quartz crystal which served as a transducer to a Kronos film thickness monitor.[20] By measuring the thickness of the deposit and coupling this with some thermodynamic considerations, a value for n_i was deducible.

The measured intensity can be calculated as follows: For the element under investigation the thickness of the deposit on the crystal, t_e, is[20]

$$t_e = \frac{(\rho_{Al})(t)}{\rho_e} \qquad \text{cm}$$

where t is the direct reading of the film thickness monitor, ρ_{Al} is the density of aluminum, for which the monitor is calibrated, and ρ_e is the density of the evaporant. The mass deposited, m_e, is

$$m_e = \frac{(\rho_{Al})(t)(\rho_c)(A_d)}{\rho_e} \quad (A_c/A_d) \qquad \text{g.}$$

where A_d is the area of the deposit and A_c is the crystal area. Not all the crystal face was coated by the impinging beam. Since the monitor was calibrated for a crystal with full active area deposit, it was necessary to increase

the actual deposit area. This explains the last factor in the previous equation.

There is an additional empirical factor, which has to do with "area pulling", that has been neglected. This factor is an outgrowth of the phenomenon that as the deposit becomes larger, the active area on the crystal is "pulled" into being the deposit area. For large enough deposits (approximately 1.1 mg/cm^2) the active and deposit areas become identical.

It was calculated in this investigation that the deposits were small enough so that the pulling factor had less than 0.5% effect and was thus ignored. We thus have

$$m_c = tA_c\rho_{Al} \qquad g.$$

To get the intensity $Y_i(0)$, we make the valid assumption that all atoms passing through the ionization plane are collected at the crystal. Then,

$$Y_i(0) = \frac{tA_c\rho_{Al}}{m\tau A_i} \qquad atoms/cm^2/sec$$

where τ is the deposit time and A_i is the cross sectional

area of the atom beam in the x-y plane at z_i.

Now n_i can still not be calculated, because it depends on T_s which is unknown. In order to determine T_s, use is made of the vapor pressure versus temperature characteristics which are known for the elements. The form of the relationship for low pressures (P < 1 Torr) is from the Clausius-Clapeyron equation[17]

$$\log P = A - B/T$$

where A and B are constants specific to the particular element. From previous analysis

$$P_s = \frac{t\rho_{Al}A_c z_i^2 M^{\frac{1}{2}}}{(1.115)(10^{22})A_s A_i m\tau} T_s^{\frac{1}{2}}$$

These two equations form a transcendental system which is best solved by graphical means, using published vapor pressure versus temperature curves.[33]

Although some concern may be raised at the accuracy of this technique, the method is less dangerous than it may first appear. What is needed here is the gas temperature only; the pressure is not explicitly necessary. The form of the log equation suggests, and the empirical

curves verify, a very sluggish temperature variation for even reasonably large variations in pressure. For the experimental operating range, an order of magnitude change in pressure produces only a 9% change in temperature. Thus, any possible error in the temperature determination is logarithmically compressed.

There is an additional compression by virtue of the square root dependence of $\bar{v}_a$ on T_s. This will further divide any small error by approximately a factor of two, so that, all in all, the accuracy of the results is maintained.

An approximate check on the data was made through the use of information about the background gas. In general, the experiments were performed with ambient pressures around the low seven scale. The same electron beam that ionized the evaporant atoms also caused some ionization of the background.

Using a subscript b to denote background, we have

$$P_b = n_b k T_b$$

$$I_b = n_b I_e l_b \sigma_b$$

where I_b is the ion current due to ionization by elec-

tron impact of background gas. Substituting,

$$I_b = \frac{I_e l_b \sigma_b P_b}{kT_b}$$

where l_b is the entire length of the ionizer (0.7cm) and $T_b \simeq 300^{o}K$.

The background was made up, in large measure, by N_2, O_2 etc. The cross sections for N^+ and O^+ are approximately $2 \times 10^{-16} cm^2$ at the relevant electron energies. Additivity measurements show that for these relatively low energies

$$\sigma_{N_2/N} \simeq \sigma_{O_2/O} \simeq 1.8 \quad .$$

Using $\sigma = 3.6 \times 10^{-16} cm^2$, a check on the measured I_b was made. The agreement was consistently within 5% for all the elements. For the approximations made here, this is quite satisfactory.

5.2 Ionization Cross Sections

The absolute ionization cross section data which were, in effect, the final results of the experiment, are presented on the following pages.

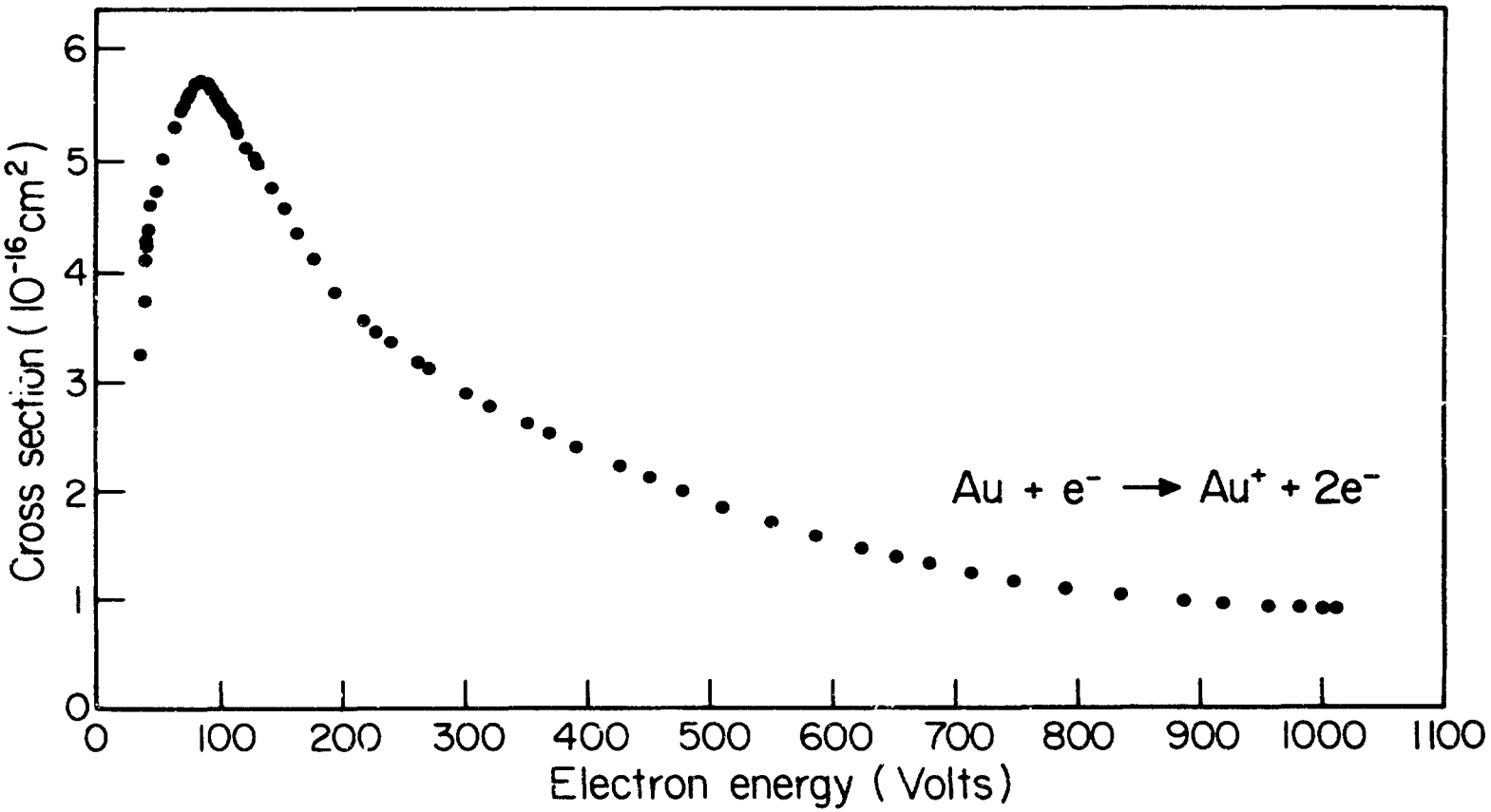

Figure 7: Cross section vs. Electron energy for Au^+.

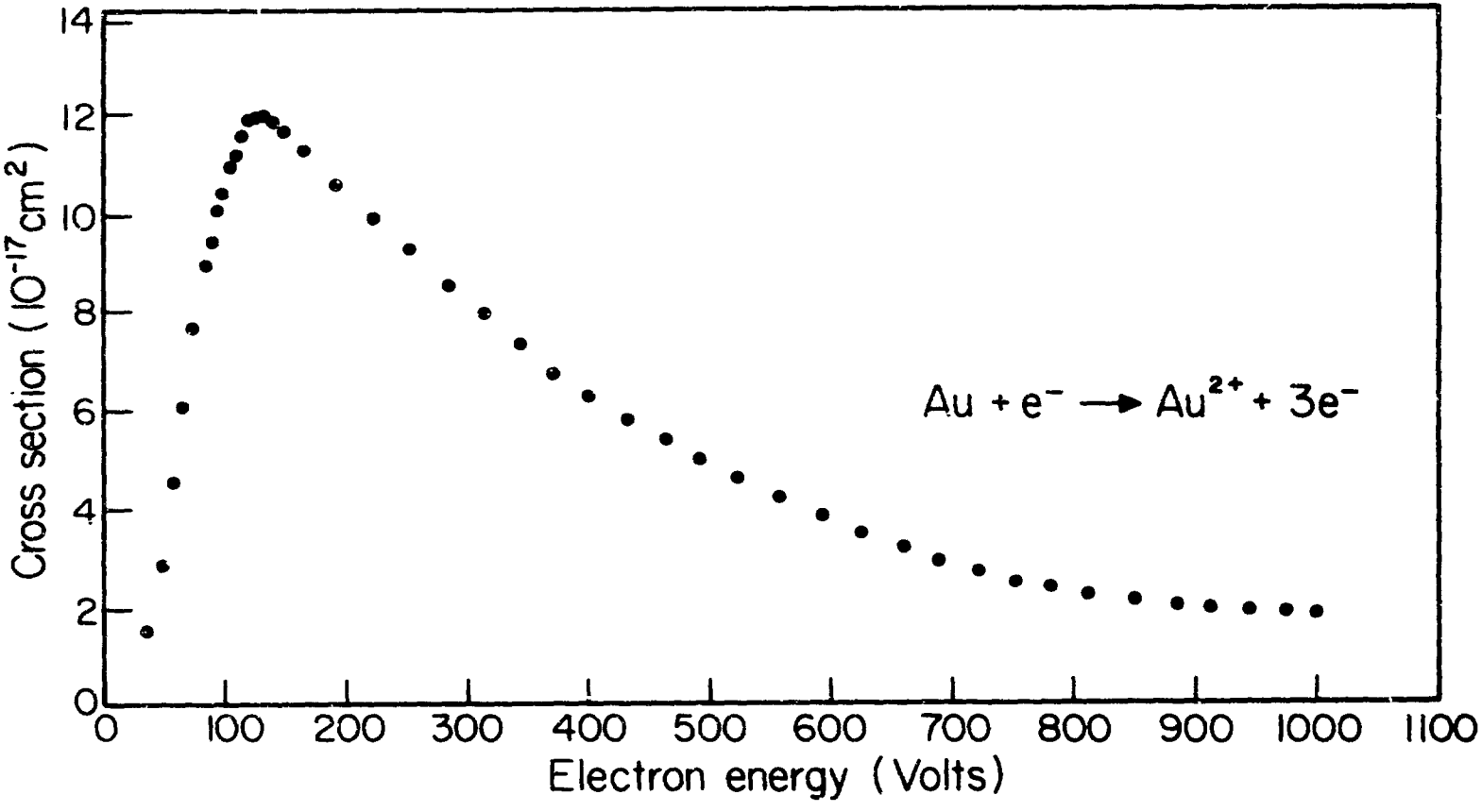

Figure 8 Cross section vs. Electron energy for Au^{2+}.

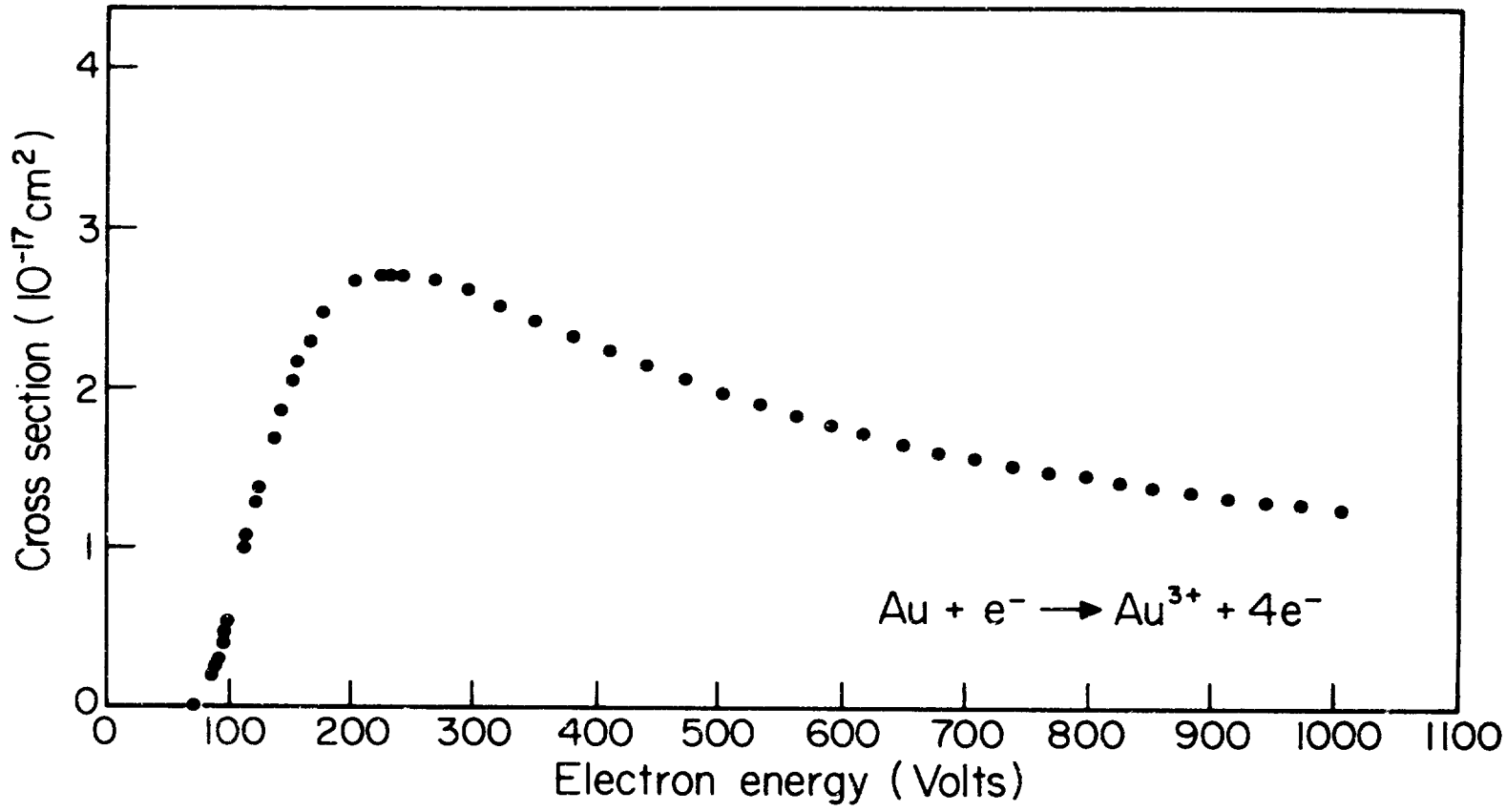

Figure 9: Cross section vs. Electron energy for Au^{3+}.

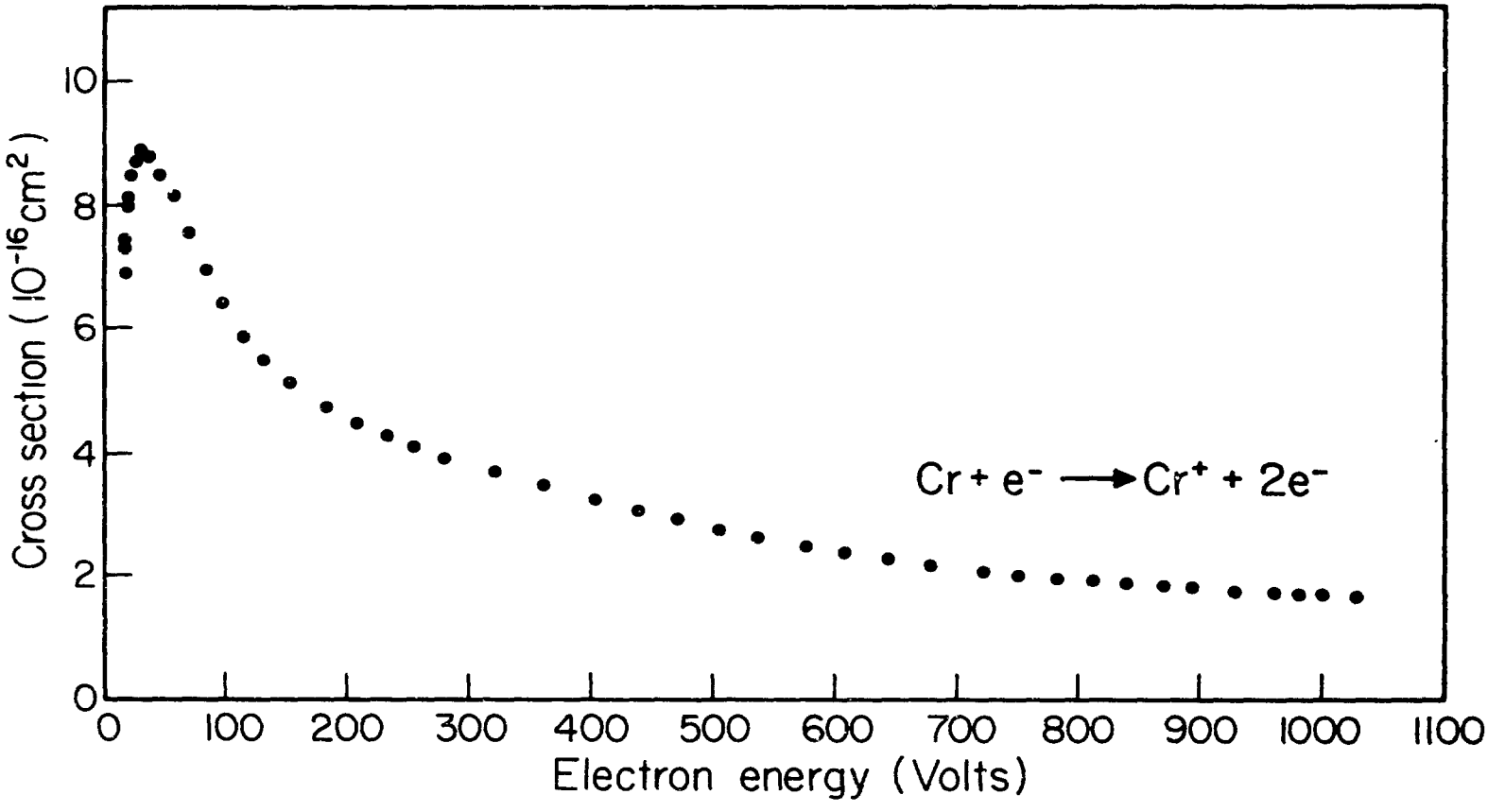

Figure 10: Cross section vs. Electron energy for Cr^+.

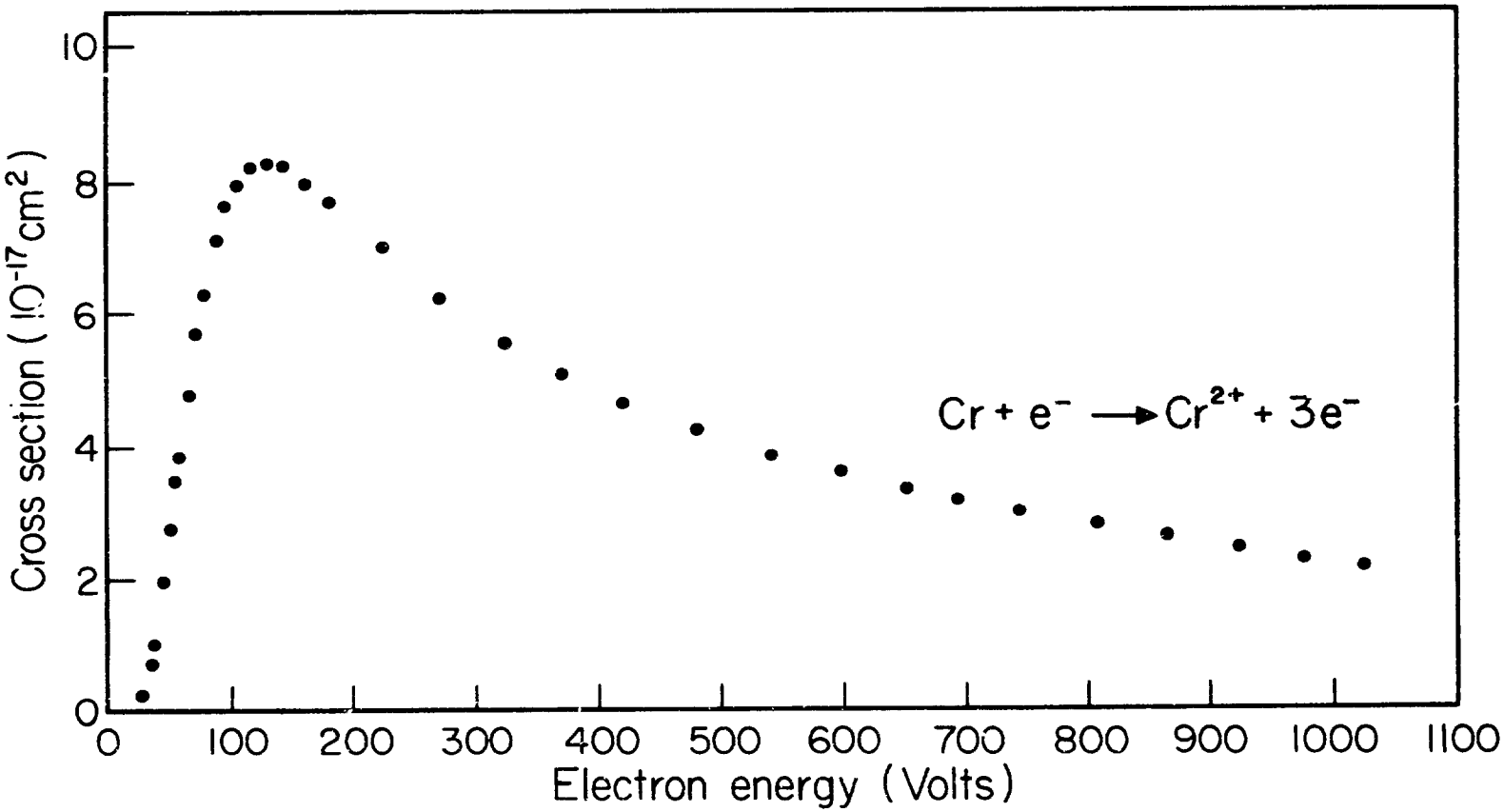

Figure 11: Cross section vs. Electron energy for Cr^{2+}.

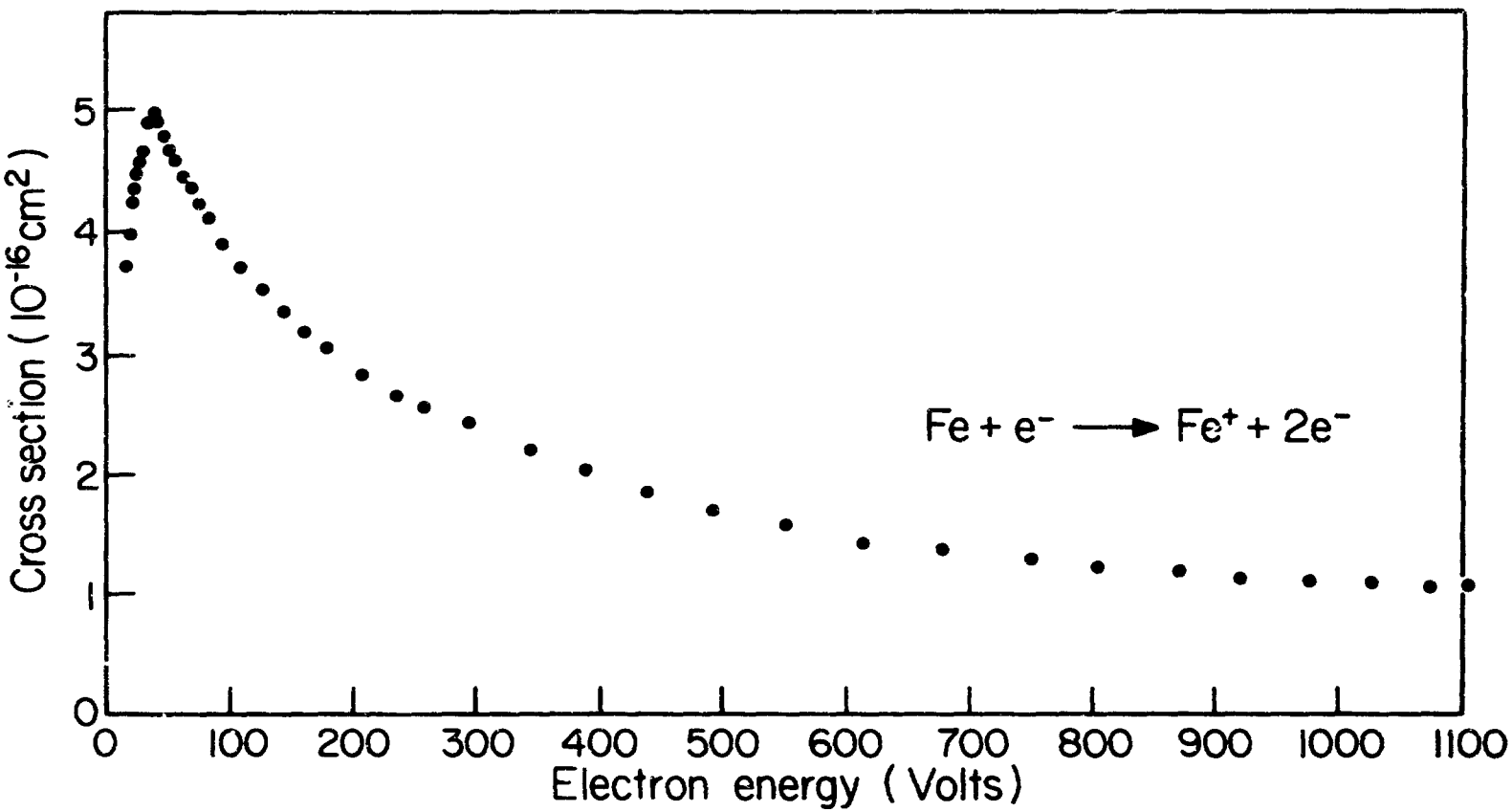

Figure 12. Cross section vs. Electron energy for Fe^+.

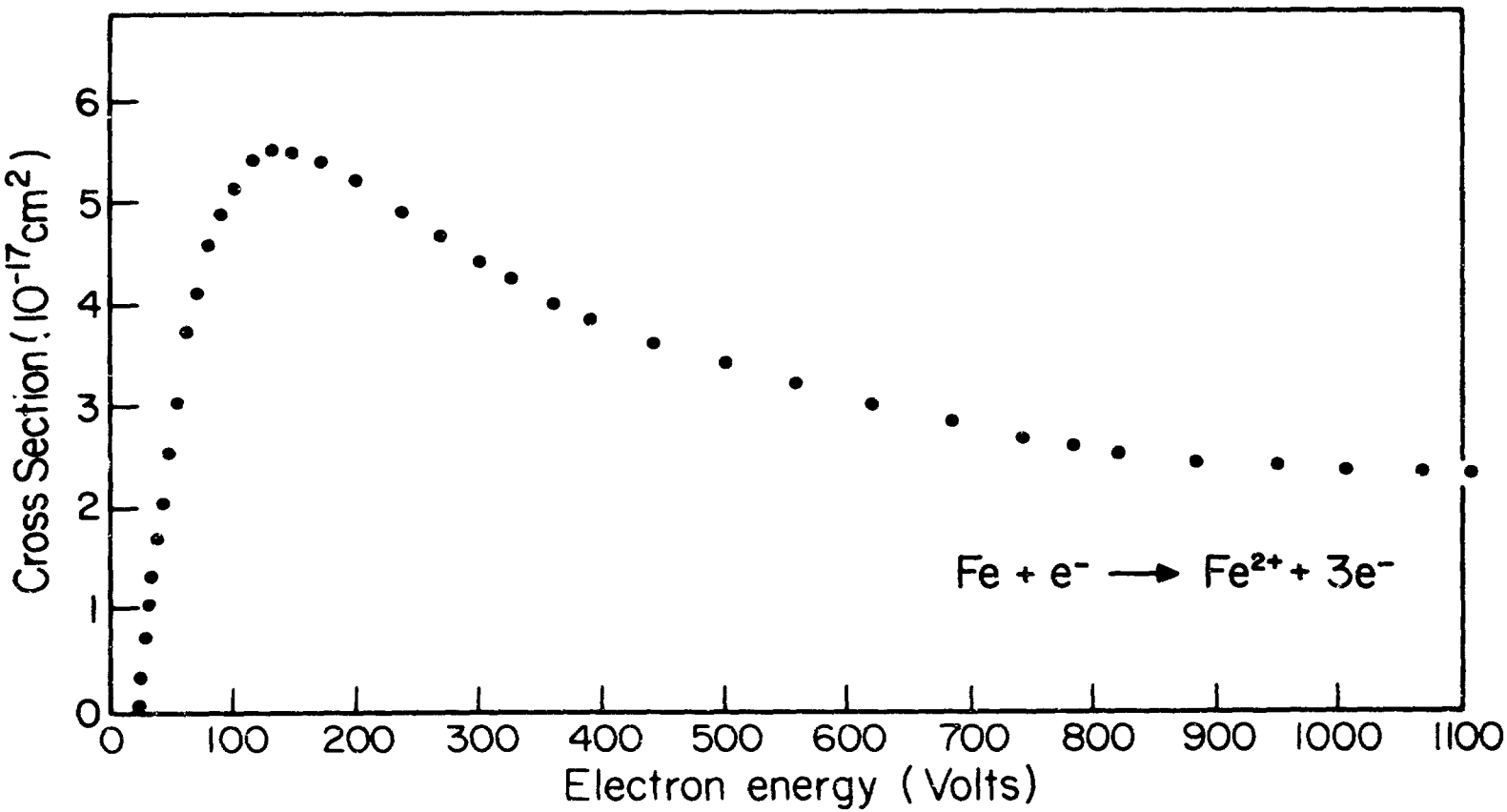

Fig. 13. Cross section vs. Electron energy for Fe^{2+}.

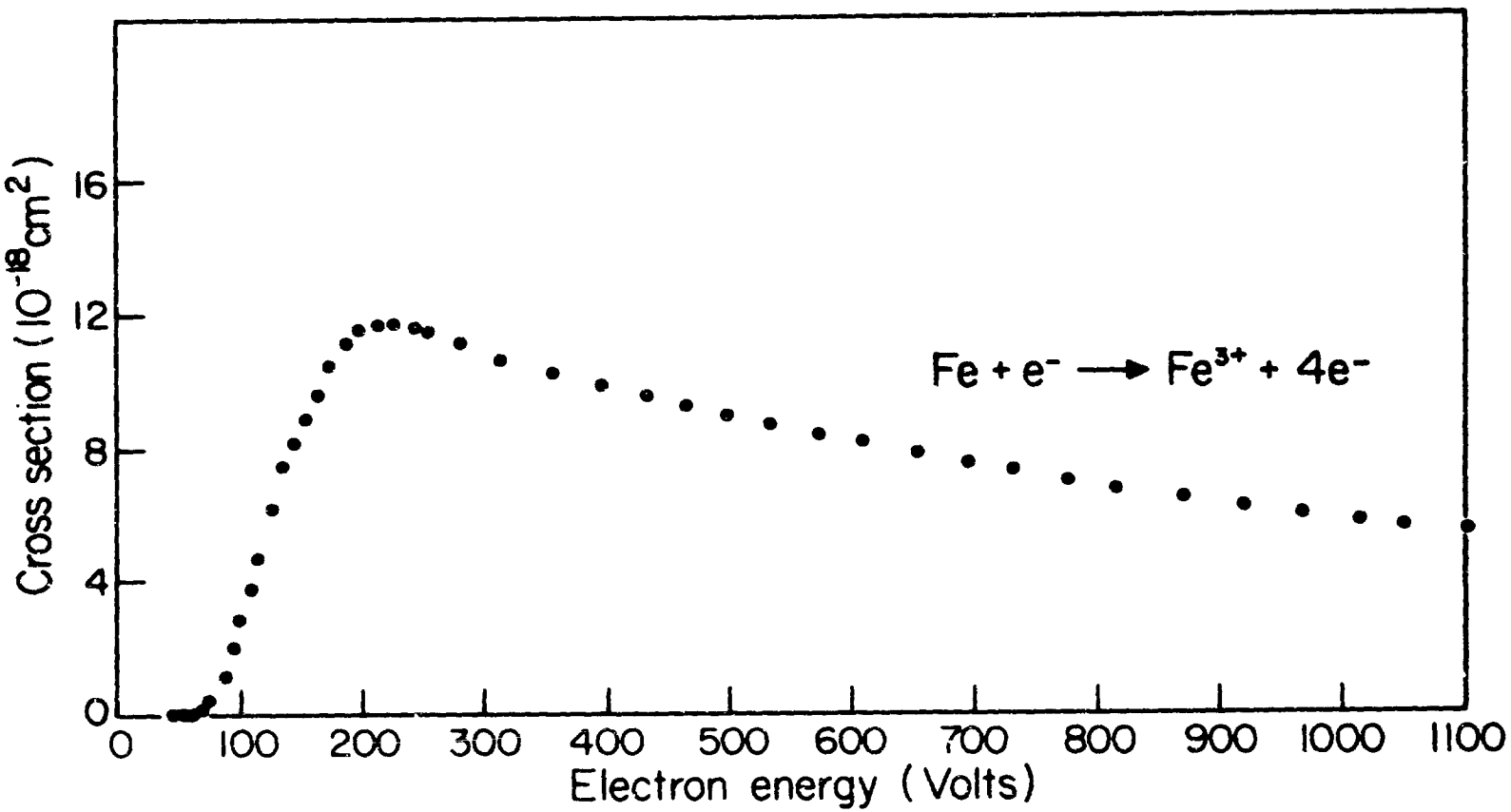

Fig. 14 Cross section vs Electron energy for Fe^{3+}.

5.3 Total Cross Sections

In theory, the total cross section is representative of the equation

$$\sigma = \sum_{k=1}^{Z} k\sigma_k$$

Because of the relatively low energy range used, and experimental limitations, as a practical matter $k \leq 3$.

In actuality, the total cross section was not measured in this investigation, and is presented here as a mathematical contrivance from the more fundamental data on the individual species. Its inclusion in this report is for purposes of comparison with some of the literature results, which deal only with the total cross section. At the time of this experiment, the only published data on the species cross section for these elements was theoretical.[5-10]

It is interesting to note that, in terms of appearance, the experimental curves actually look better than the mathematically derived ones. This is due partially to the graphical technique that was used in their construction. Had the digital data been used instead, the results would probably have been somewhat improved.

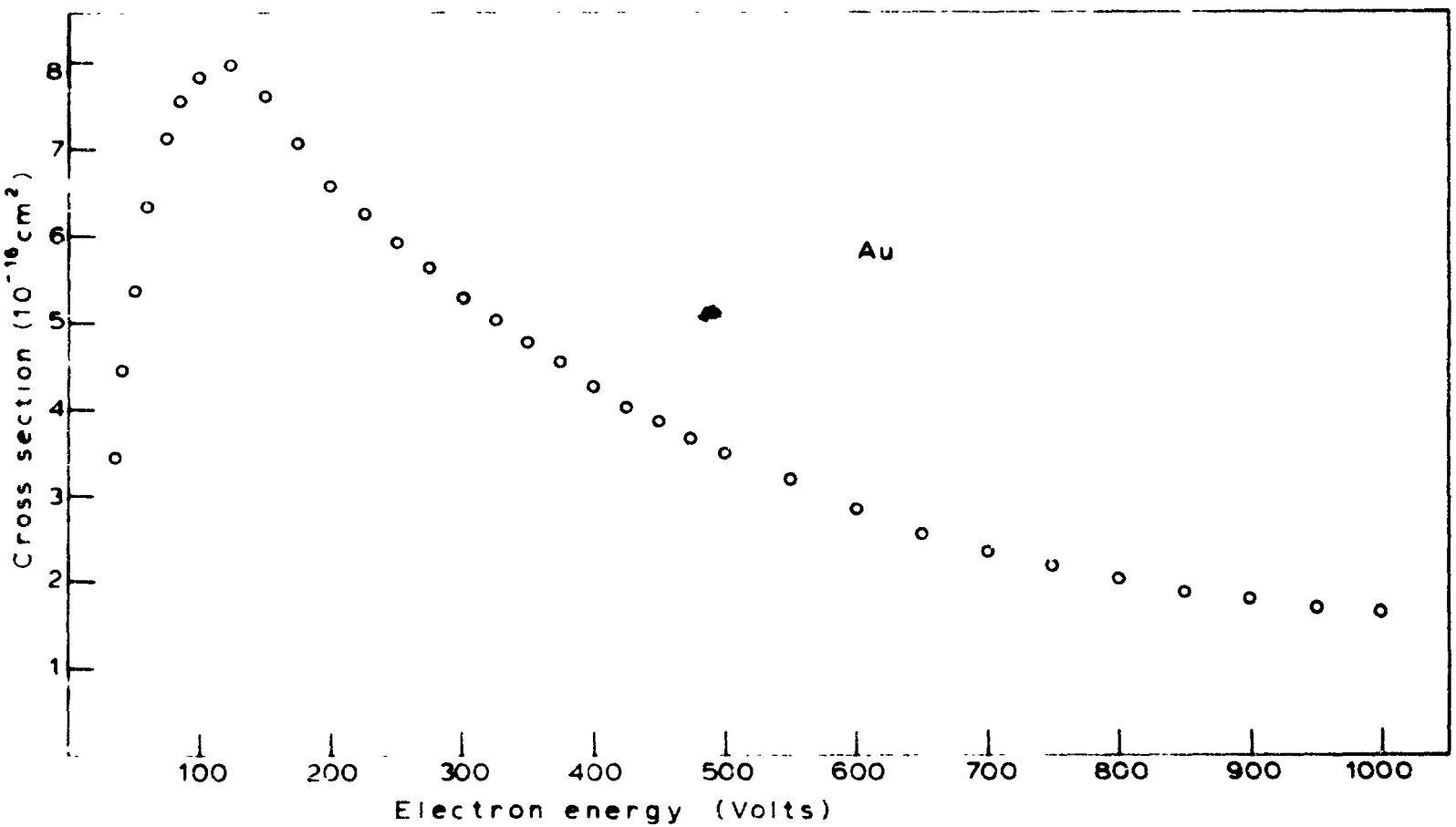

Figure 15: Total cross section vs. Electron energy for Au.

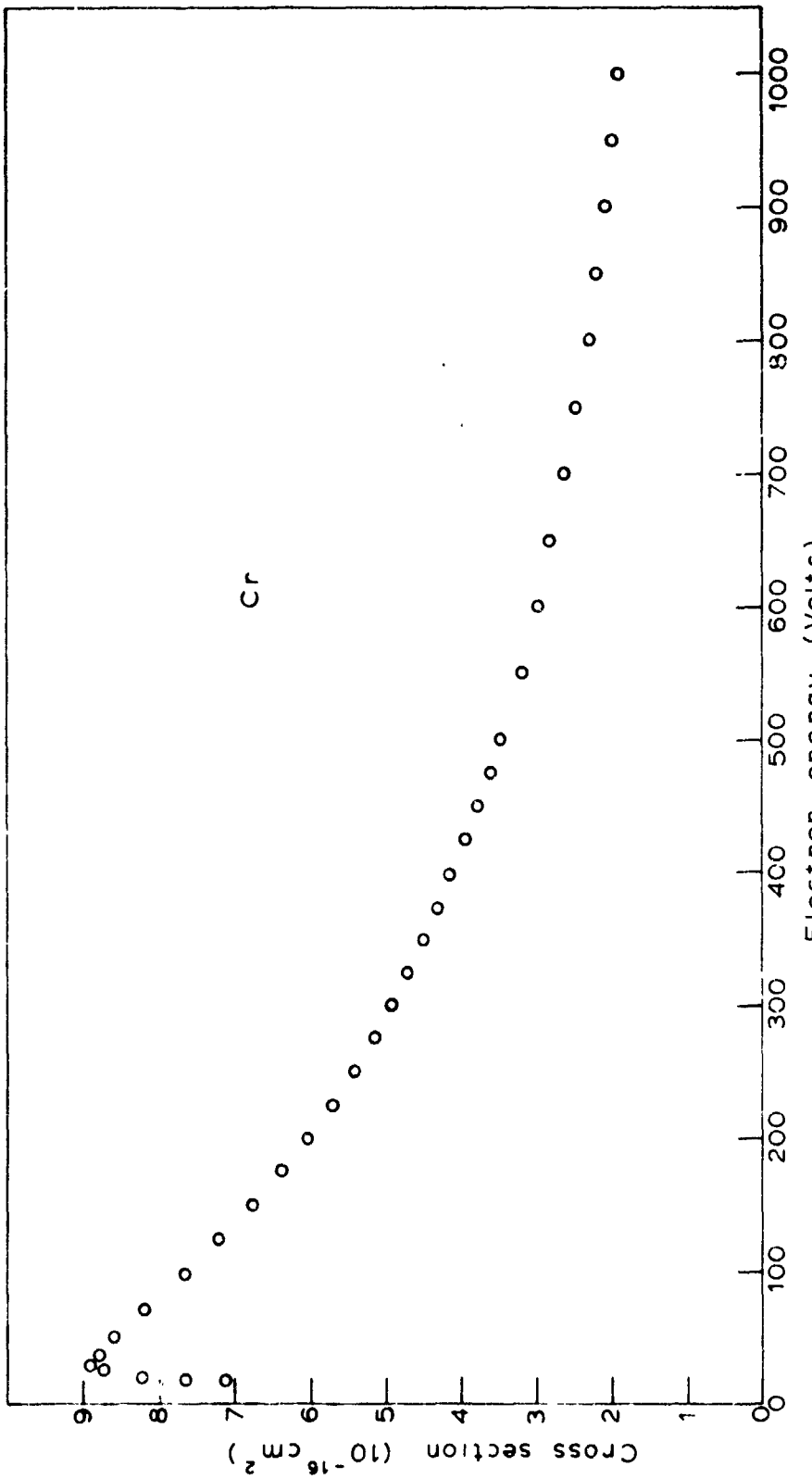

Figure 16: Total cross section vs. Electron energy for Cr.

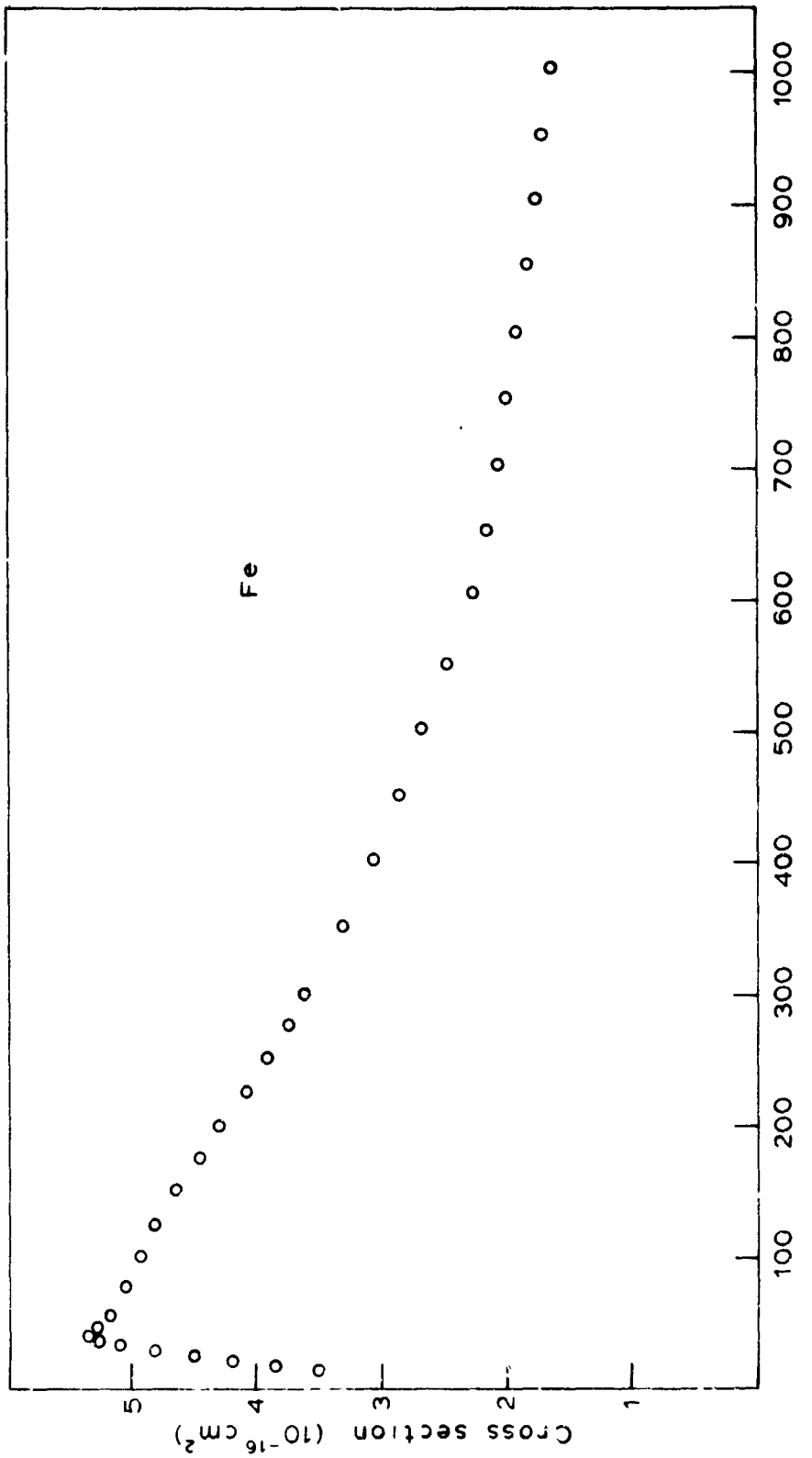

Figure 17. Total cross section vs. Electron energy for Fe.

5.4 Literature Comparison

Schroeer, et al[1], have been responsible for the only reported absolute data on Au. Theirs is a discussion of the total cross section, which they found peaked at 100 eV. and had a value of $\sigma(Au) = 15.3 \times 10^{-16}$ cm^2. This compares with the peak result of of this investigation where $\sigma(Au) = 7.92 \times 10^{-16}$ cm^2 at 125 eV. It should be noted that Schroeer, et al, also presented $\sigma(Cu)$ in the same paper and compared it favorably to Crawford's[2] data multiplied by 1.85. If the same manipulation is applied to Au, similar results obtain here, as the form of the two data curves is about the same. The ratio of peak values is 1.93. At 100 eV. the ratio is 1.95.

Compared to Crawford's[2] results on copper, $\sigma(Au)/\sigma(Cu) = 1.92$. Schroeer's ratio is 2.0, Ackerman, et al's[3,9], is 1.9 or 2.1 at 70 eV.

A derived value from Ackerman[3] based on argon and Otvos and Stevenson's[4] relative cross sections is given by Pottie[5] as $\sigma(Au) = 11.6 \times 10^{-16}$ cm^2 at 75 eV.

There appears to be no experimental literature on the specie cross sections, and the theoretical determinations have a wide range of forecast depending

on the approximations made. Thus, for example, Lotz[6] gives a single ionization cross section peak of $\sigma(Au^+) = 5.0 \times 10^{-16}$ cm^2 at 70 eV. Mann's[7] results yield $\sigma(Au^+) = 6.46 \times 10^{-16}$ cm^2, and Lin and Stafford[8], with a more classical derivation, conclude that $\sigma(Au^+) = 13.3 \times 10^{-16}$ cm^2. at about 80 eV.

No direct experimental determinations of absolute cross sections for Cr and Fe appear in the literature. Thus, the discussion of results in this area must be confined to comparisons of ratios of relative data. Using ratios eliminates the constants of proportionability between relative and absolute data on specific elements and allows for at least a cursory examination of previous results.

In this investigation, $\sigma(Fe)/\sigma(Au) = 0.83$ at 60 eV. and 0.96 at 50 eV.

Cooper, et al,[10], present this ratio as 0.97. Comparing the Fe data in this report with Crawford and Wang's[11] Ag results yields $\sigma(Fe)/\sigma(Ag) = 0.97$, compared to Cooper's[10] average value of 0.99.

$\sigma(Cr)/\sigma(Au) = 1.22$ at 70 eV., from the data here, which compares with Ackerman, et al.'s[12] ratio of 1.5. The same source reports $\sigma(Cr^{++})/\sigma(Cr^+) = 0.03$ at 70 eV.

This appears to be low, as the ionization potential for Cr^{++} is 16.6 V., and one expects about one order of magnitude reduction in cross section peak height between single and double ionization. By the time the electron energy is as high as 70 eV., $\sigma(Cr^{++})$ should no longer be negligible and a larger ratio would be expected. It was found here that $\sigma(Cr^{++})/\sigma(Cr^{+}) \approx 0.075$.

Error Analysis

Uncertainties in the experiment arose in the usual considerations of instrument stability, which was within ±1.5%. Then there was a ±1% randomness in the transmission of atom and electron beams through the ionizer. Beam control feedback limited drifts in the beams to about 2%, and stray effects such as particle scattering and structural alignment were less than 1%. The precision of the relative cross section data, therefore, was good to within ±3%.

Absolute measurements, however, generated additional vagaries. Area pulling in the film thickness monitor introduced an uncertainty of ±0.5%. Because of the variations in velocities, differences in

spectrometer transmission by specie may have resulted. High V_{IE} and V_{ID} tended to reduce this to ±2%. Ion current measurement was upset by the background gas and contained an error of about ±4%. The particle counting technique virtually eliminated any fluctuations of yield by specie at the conversion dynode. All things considered then, the absolute measurements were precise within ±9%.

5.5 Multiple Ion Formation

It is clear in the case of single ion formation that ionization is a one-step process described by the reaction

$$Au + e^- \rightarrow Au^+ + 2e^-$$

When higher orders of ionization are involved, however, it is no longer necessarily obvious exactly what mechanism is responsible for the multiple ion formation. In particular, consider the case of doubly ionized gold. Two possible reaction routes are possible:

$$Au + e^- \rightarrow Au^{2+} + 3e^-$$

Or:

$$Au + e^- \rightarrow Au^+ + 2e^-$$

$$Au^+ + e^- \rightarrow Au^{2+} + 2e^-$$

In this section a semi-empirical order of magnitude analysis is presented to show that the single collision reaction is indeed the way gold achieves a double ionized status. The specific consideration here is with Au^{2+}, but it can be shown that a similar result obtains for Fe or Cr and for any other multiply-charged ion.

By way of notation, it is necessary to differentiate

between ion currents and ion counts. In order to do this, the letter I with a subscript will be used to indicate a true ion current whereas a superscript will designate an ion count. The species of ion will also be included in the script notation.

The total ion current I_{Au} for gold was measured at $V_{EA} = 100V$.

$$I_{Au} = I_{+} + I_{2+} + I_{3+} \ldots \sim 10^{-11} \text{ A.}$$

The ratios of I_{3+}/I_{+} and I_{2+}/I_{+} may be obtained by examining the cross section plots for singly, doubly and triply charged gold. It must be noted that the method of measurement in this investigation leads to data on the number of ions of specie produced. In order to transform this into a current, the number of ions must be multiplied by the charge on each ion. Thus

$$I_{+} = I^{+}$$

$$I_{2+} = 2I^{2+}, \text{ etc.}$$

Then

$$I_{Au} = I_{+} + (I_{2+}/I_{+})I_{+} + (I_{3+}/I_{+})I_{+}$$

$$= I_+ + (2)\ (I^{2+}/I_+)I_+ + (3)\ (I^{3+}/I_+)I_+.$$

For gold, the empirical ratio's at 100V. are

$$\frac{I^{2+}}{I^+} = .193 \qquad \frac{I^{3+}}{I^+} = .011$$

and considering total current

$$I_+ \sim 5 \times 10^{-12}\ \text{A.}$$

Orders of ionization higher than three are assumed negligible.

Now $I_+ = \frac{\Delta q_+}{\Delta t}$ and each ion bears a unit electronic charge of 1.6×10^{-19} coul. So the number of Au^+ ions collected per second is

$$N_+ = \frac{I_+}{1.6 \times 10^{-19}} \sim 3 \times 10^7$$

Under the assumption that virtually all ions that cross the entrance aperture of the collector are recorded as collected current, N_+ is the same as the number of ions emerging from the ionization chamber and impinging on the collector.

The number of atoms of gold per unit area per unit time in the original atomic beam was measured by a film

thickness monitor to determine the neutral density. The result was

$$N_o \sim 10^{15} \text{ atoms/cm}^2\text{/sec.}$$

One can then deduce a probability of ionization to the singly charged state as

$$p(Au \rightarrow Au^+) = \frac{N_+}{N_o} \sim 3 \times 10^{-8}$$

We now make the assumption

$$p(Au^+ \rightarrow Au^{2+}) = p(Au \rightarrow Au^+)$$

That is, in a statistical sense the electron beam does not differentiate between a neutral atom and an ion in its path. (This assumption is not strictly true, and the ramifications of making it are discussed subsequently.)

This means

$$p(Au \rightarrow Au^{2+}) = (N_+/N_o)^2 \sim 10^{-15}$$

Since there are 10^{15} atoms/cm^2/sec. it follows that approximately 1 atom/sec. would undergo such a double collision. This amounts to a double ion current of

$$I_{2+} \sim (1)\ (2)\ (1.6)\ (10^{-19}) = 3 \times 10^{-19}\ \text{A.}$$

double collision

But the actual double ion current contribution is

$$I_{2+} = 2(I_{2+}/I_{+})I_{+} \sim 2 \times 10^{-12}\ \text{A.}$$

Thus, the percent of Au^{2+} current contributed by double collisions is approximately

$$F_{d2+} \sim (10^{2})\ (3 \times 10^{-19}/2 \times 10^{-12}) \sim 10^{-5}\%$$

Evaluation of Assumptions:

1) Orders of ionization higher then three are negligible. Fourth order ionization for gold was virtually undetectable under conditions of this investigation. This means that Au^{4+} was less than 1% amplitude of Au^{+} even at maximum. At the relatively low energy of this calculation (V_{EA} = 100v). Au^{4+} would be an order of magnitude below that.

2) Complete collection of ions. This is necessary for the basic experiment to be successful and was manifest in a saturation effect. Beyond a certain draw out voltage V_{ID} and shield voltage V_{ES} there was

no increase in collected ion current - indicating that all ions were being collected and that only positive charges were being considered in the current.

3) $p(Au^+ \rightarrow Au^{2+}) = p(Au \rightarrow Au^+)$. For the probabilities to be truly equal, there must be indistinguishability between Au and Au^+ in two senses: first with respect to particular forces present in the region and second with respect to the electron beam.

Because there are electric fields in the ionization chamber, the ions are subjected to different forces than are the neutrals. The effect of the fields is to alter the trajectories of the ions. Also, the ionized state of the particle changes the cross section target for the oppositely charged electron. Both these factors tend to enhance the probability of a second ionization. On the other hand, the assumption of equal probability of collision events ignores the fact that the first ionization need not take place near the entrance of ionization chamber. The consequent lack of remaining time in traversal would tend to reduce the probability of a subsequent collision. Furthermore, all numbers have been shaded

on the conservative side to enhance the probability magnitudes.

In any event, these effects are nowhere near the several orders of magnitude required to alter the preceding conclusion. It remains demonstrated that double ionization is a one step process.

REFERENCES

1. J. M. Schroeer, D. H. Gunduz, S. Livingston, J. Chem. Phys. 58, 5135 (1973)

2. C. K. Crawford, "Electron-Ionization Cross Sections", Tech. Rept. 1, Particle Optics Lab, M.I.T. (1967), AFML TR-67-376 (AD 826983)

3. M. Ackerman, F.E. Stafford, J. Drowart, J. Chem. Phys. 33,1784

4. J.W. Otvos, D.P. Stevenson, J. Am. Chem. Soc. 78,546 (1956)

5. R.F. Pottie, J. Chem. Phys. 44,916 (1966)

6. W. Lotz, Z. Phys. 232,101 (1970)

7. J.B. Mann, J. Chem. Phys. 46,1646 (1967)

8. S.S. Lin, F.F. Stafford, J. Chem. Phys. 48,3885 (1968)

9. M. Ackerman, J. Drowart, F.F. Stafford, G. Verhagen, J. Chem Phys. 36,1557 (1962)

10. J.L. Cooper, G.A. Pressley, F.F. Stafford, J. Chem. Phys. 44,3946 (1966)

11. C.K. Crawford, K.L. Wang, J. Chem. Phys. 47,4667 (1967)

12. M. Ackerman, F.F. Stafford, G. Verhaegen, J. Chem. Phys. 36,1560 (1962)

13. J.C. Helmer, F.B. Jacobs, P.A. Sturrock, J. Chem. Phys. 31,458 (1960)

14. G.R. Hanes, J. Chem. Phys. 31,2171 (1960)

15. N.F. Ramsey, Molecular Beams, Oxford Press (1956)

16. N.F. Mott, H.S.W. Massey, Theory of Atomic Collisions, Oxford Press (1965)

17. S. Dushman, J.M. Lafferty (ed.), Scientific Foundations of Vacuum Technique, Wiley (1962)

18. C.F. Woodward, Development of a Quadrupole Mass. Spectrometer, PhD. Thesis, E.E. Dept., M.I.T. (1964)

19. J.R. Pierce, Theory & Design of Electron Beams, D. Van Nostrand (1949)

20. Operations and Service Manual, QM-300 Series Film Thickness Monitor, Rev. A, 11/72, Kronos Inc., 1647-7 W. Sepulveda Blvd., Torrance, Calif. 90501

21. V.W. Hughes, H.L. Schultz (ed.), Methods of Experimental Physics, Vol. 4A, Academic Press (1967)

22. H.S.W. Massey, E.H.S. Burhop, H.B. Gilbody, Electronic & Ionic Impact Phenomena, Vol. 1, Clarendon Press (1969)

23. E.W. McDaniel, Collision Phenomena in Ionized Gases, Wiley (1964)

24. L.J. Kieffer, G.H. Dunn, Reviews of Mod. Phys., 38,1 (1966)

25. L.J. Kieffer, Bibliography of Low Energy Electron Collision Cross Section Data, NBS Miscellaneous Publications, 280 (1967)

26. K.L. Wang, M.D. Brody, C.K. Crawford, Electron Impact Ionization Cross Sections, Tech. Rept. AFML-TR-69-5, Wright-Patterson AFB, Ohio (M.I.T. Particle Optics Lab TR-3) (1969)

27. K.L. Wang, C.K. Crawford, Electron Impact Ionization Cross Sections, Tech. Rept. AFML-TR-70-289, Wright-Patterson AFB, Ohio (M.I.T. Particle Optics Lab TR-6) (1971)

28. A. Smith, Notes on the Performance & Application of EMI Windowless Particle Detectors, EMI R/P034

29. W. Davenport, W. Root, Introduction to the Theory of Random Signals and Noise, McGraw-Hill (1958)

30. P. Grivet, Electron Optics, Pergamon Press (1972)

31. J.C. El-Kareh, A. El-Kareh, Electron Beams, Lenses and Optics, Academic Press, (1970)

32. E.H. Kennard, Kinetic Theory of Gases, McGraw-Hill (1938)

33. R. Honig, Vapor Pressure Data for the More Common Elements, RCA Rev. 18, 195-204 (June 1957)

34. W.A. Coughlan, R.E. Clausing, Atomic Data, Vol. 5 #4,318 (1973)

35. C.C.Lu, T.A. Carlson, F.B. Malik, T.C. Tucker, C.W. Nestor, Jr., Eigenvalues, Radial Expectation Values & Potentials for Free Atoms from Z = 2 to 126 as calculated from Relativistic Hartree-Fock-Slater Atomic Wave Functions, Oak Ridge National Lab Report, ORNL-4614 (1970)

36. L. Holland, Vacuum Deposition of Thin Films, Wiley (1956)